Composite Structures 132 (2015) 1274–1287

Contents lists available at ScienceDirect

Composite Structures

journal homepage: www.elsevier.com/locate/compstruct

An exact spectral-dynamic stiffness method for free flexural vibration analysis of orthotropic composite plate assemblies – Part I: Theory

X. Liu *, J.R. Banerjee

School of Mathematics, Computer Science and Engineering, City University London, London EC1V 0HB, UK

ARTICLE INFO

Article history:
Available online 17 July 2015

Keywords:
Spectral-dynamic stiffness method (S-DSM)
Composite plate assemblies
Free vibration analysis
Arbitrary boundary conditions
Enhanced Wittrick–Williams algorithm

ABSTRACT

A spectral-dynamic stiffness method (S-DSM) for exact free vibration analysis of general orthotropic composite plate-like structures is presented in the paper. The method combines the advantages of the classical dynamic stiffness method (DSM) with those of the spectral method, and it resembles the finite element and the boundary element methods. The formulation is based on the exact general solution of the governing differential equation, which provides complete flexibility to describe any arbitrary boundary conditions. The dynamic stiffness formulation is essentially accomplished through a mixed-variable approach in a symbolic form with explicit expressions rendering physical meanings. Then a systematic procedure for plate assemblies under arbitrary boundary constraints is described. Finally, a set of novel techniques are proposed to enhance the Wittrick–Williams algorithm by resolving the fully-clamped plate problem. The validation of the theory and its applications to a wide range of engineering structures are demonstrated in Part II of this two-part paper.

1. Introduction

Composite structures are increasingly being used in areas of aerospace, civil, naval, automotive, electronic, and armoured engineering amongst others. In many cases, complex engineering structures are modelled by composite plates and their assemblies subject to arbitrarily prescribed boundary conditions. In this respect, free vibration analysis is an essential consideration in each stage of such structures during design, manufacturing, operation and maintenance. Thus an accurate and efficient method to compute natural frequencies and mode shapes of composite structures is important. Furthermore, some areas like structural health monitoring and active control of vibration and noise require accurate knowledge of free vibration behaviour both in the low and high frequency range, warranting the development of more accurate and robust methods. It should be noted that the finite element method can become unreliable in vibration analysis at high frequency ranges, for example, cutting tools at ultrasonic frequencies.

Against this background, the first part of this paper is aimed at developing an efficient and robust method for exact free vibration analysis of composite plate-like structures for any arbitrary boundary conditions within any frequency range. This method is termed as the spectral-dynamic stiffness method, abbreviated as S-DSM. The S-DSM is mainly based on the methodology of both the dynamic stiffness method (DSM) and the spectral method (SM). As a consequence, it has the merits of both methods. Furthermore, the S-DSM shares some important advantages of the finite element method (FEM) and boundary element method (BEM), but does not have any of their disadvantages. Table 1 shows the main features of the current S-DSM side by side to those of the conventional FEM and DSM. The differences and similarities are self-explanatory in the table.

The current S-DSM inherits all the advantages of the classical DSM such as high accuracy, computational efficiency and the certainty that no natural frequencies of the structure is missed. Understandably the S-DSM and DSM have much superior modelling capability over the FEM and other methods. This is mainly due to three reasons: (i) The dynamic stiffness (DS) matrix is formulated from the strong form solution of the governing differential equation (GDE) and boundary conditions (BC). Therefore no discretisation is needed except when geometric and/or material discontinuities in the structure occur. Consequently, the DSM and S-DSM give exact solutions with high computational efficiency. This is in sharp contrast to the usual FEM and BEM whose shape functions are generally approximate and both can be computationally expensive when higher natural frequencies and/or better accuracies are required, (ii) The DSM and S-DSM are versatile because the DS matrix can be assembled in the same way as the FEM, (iii) Natural frequencies are computed by applying the Wittrick–Williams algorithm on the DS matrix. This algorithm is robust and it ensures that no natural frequency of the structure is missed.

* Corresponding author.
E-mail address: xiangliu06@gmail.com (X. Liu).

http://dx.doi.org/10.1016/j.compstruct.2015.07.020
0263-8223/

Table 1
Comparisons of the FEM and the DSM with the current S-DSM for free vibration problems. For notational convenience, some abbreviations are introduced: GDE – Governing differential equation; BC – Boundary conditions; DOF – degree(s) of freedom; SF – shape function(s).

	Conventional FEM	DSM (SEM)	S-DSM
Mathematical basis	Variation based	Differentiation based (strong form)	Differentiation based (strong form)
Methodology	Uses approximate shape functions to describe the displacement field; Relies on a variational formulation to derive the elemental stiffness and mass matrices; Assemble for the whole structure; Apply BC and solve	Obtain exact general solution of GDE; Substitute it into BC to form elemental DS matrix; Assemble the DS matrices for the whole structure; Apply BC and solve	Obtain exact general solution of GDE in spectral sense (both in time and in space); Uses a set of novel techniques to make the method numerically stable and efficient; The rest steps are similar to the DSM
h-refinement [1] (finer mesh)	Fine mesh is needed, depending on the required accuracy and/or for the highest natural frequency	Extremely coarse mesh is adequate for exact solutions unless geometric and/or material discontinuities occur	Same as the DSM
p-refinement [1] (higher SF order)	Only low order polynomials are adopted	N/A (only allows sinusoidal deformation)	Space-wise spectral refinement, SF order can be as high as possible (numerically stable)
Shape functions (SF)	Approximate and frequency independent	Exact frequency dependent (spectral in time only)	Exact frequency–wavenumber dependent (spectral both in time and in space)
Assembly	Assemble directly to allow complex geometries: compatibility, continuity and equilibrium are generally satisfied	Assemble directly, but limited to one-directional (prismatic) assembly	Assemble directly to allow complex geometry: the compatibility, continuity and equilibrium are automatically satisfied
Arbitrary boundary conditions (BC)	Yes, approximately applied at the boundary point nodes	No, limited to Levy type plates with sinusoidally varied boundary conditions only	Yes, directly and accurately applied using linear transformation
Final eigenvalue matrix(ces)	Two frequency-independent/symmetric/sparse matrices for mass and stiffness properties	One frequency-dependent/symmetric/dense (sparse for large assembly) DS matrix	Same as the DSM
Solver	Generally linear eigenvalue solvers	The Wittrick–Williams algorithm	The Wittrick–Williams algorithm
Computational cost	Expensive especially when higher natural frequencies and/or higher accuracies are required	Inexpensive	Inexpensive
Natural frequencies	May miss some	Impossible to miss	Impossible to miss
High frequencies computation	Difficult, if not impossible	Possible but has been difficult so far for plate and shell problems	No problem, robust and efficient

The DSM was pioneered by Kolouˇsek [2] in the 1940's, but it was not until the development of the Wittrick–Williams (WW) algorithm [3] in the seventies when the DSM became popular and entered into a sustained period of prosperous developments. In the past four decades numerous exact DS theories have been proposed for a wide range of one-dimensional (1D) elements such as bars and beams for which Banerjee et al. [4–9] have been leading promoters. However, when developing two dimensional (2D) DS elements like plates, two serious limitations emerged for classical application of the DSM.

(i) First, the DSM was restricted to Levy-type rectangular plates with one pair of opposite edges simply supported. Thus, it allowed only sinusoidal deformation in one direction (e.g., see [10–15]) which brought two inevitable consequences. On the one hand, it is undoubtedly an obstacle in applying more general boundary conditions. On the other hand, the Levy-type solution restricted the application only to one-directional plate assemblies and there was no clear possibility of assembling dissimilar elements like beams and bars. These are naturally serious restrictions because engineering structures are modelled as plate and other elements assemblies in a quite general manner.
(ii) Additionally, it should be emphasised that in almost all of the previous DSM developments on plates [10–15], one of the key issues in the WW algorithm application was the evaluation of the natural frequencies of fully-clamped plate elements, which can sometimes be very difficult.

The challenges encountered in solving the first aforementioned restriction lie in obtaining a general solution of the plate differential equation in free vibration. Such a general solution should not only satisfy the 2D GDE rigorously but also must provide accurate representation for arbitrarily prescribed BC on the four edges of the plate. This is resolved in this paper by using the concept of spectral method (SM) [16,17], which is indicated by the letter 'S' for the current method S-DSM. It should be noted that the term *spectral* in the current S-DSM is used in both *time-wise* and *space-wise* sense, which is somehow different from the spectral element method (SEM) used by many, see Patera [18], Ostachowicz et al. [19] and Lee [20] for examples. In [18,19], *spectral* of SEM is used only for spatial coordinates and the *spectral* in [20] by Lee is only for time coordinate. In this paper, the *time-wise* Fourier transform (spectral) of the time coordinate will be referred to as *frequency* whereas the space-wise Fourier transform (spectral) of the spatial coordinates is denoted as *wavenumber*.

The second limitation mentioned above has been completely removed in the research by an elegant technique inspired by the Gauss circle problem [21] in conjunction with the use of a mixed-variable formulation for the DS matrix. This methodology enhances the WW algorithm significantly and makes the current S-DSM efficient and robust within any frequency range covering low to high frequencies.

The methodology of the S-DSM is somehow different from that of the FEM (see Table 1) and some technical preliminaries are required to show the steps used in the development of the S-DSM.

(i) The *time*-dependent plate vibration problem governed by the GDE is first transformed into *frequency* dependent GDE by using harmonic oscillation assumption (Section 2.1). Then the general solution is represented as a superposition of two series solutions, which are deduced analytically based on the idea of the spectral method [16,17] applied in the *spatial* domain. The general solution is then partitioned into four symmetric and antisymmetric component cases (Section 2.2). Accordingly, the BC are partitioned into four symmetric and antisymmetric components as described in Section 2.3.
(ii) Then in Section 3.1, a symbolic, but concise derivation is carried out through a mixed-variable formulation with unified notations leading to DS component matrices. (The formulation also facilitates the application of the enhanced WW algorithm introduced later.) In the light of the partitioning of the BC, the analytically formulated DS component matrices are superposed to form the DS matrix of the complete orthotropic composite plate element for the general case (Section 3.2).
(iii) Following analogous procedure as used in the FEM, the overall DS matrix of a plate assembly is modelled by assembling the DS matrices for each individual plate elements (Section 4.1).
(iv) The overall DS matrix now satisfies the GDE exactly in the whole domain, which also allows the application of any arbitrary BC accurately, see Section 4.2.
(v) The natural frequencies of the plate structure are extracted through the application of the WW algorithm enhanced significantly in this paper by using novel techniques. Mode shapes are computed using a slightly different procedure when compared with that of the classical DSM, see Section 5.

It is now appropriate to review briefly some of the other typical analytical and semi-analytical attempts made for free vibration analysis of plates. These include the Rayleigh–Ritz method [22–25], Fourier series-based analytical method [26–29] and superposition method [30–32] amongst others [33–36]. The Rayleigh–Ritz method has been frequently used [22–25] because of its flexibility and conceptual simplicity [37]. However, different admissible functions should be chosen for different boundary conditions so that the formulation using the Rayleigh–Ritz method is not unique. Recently, a Fourier-series based analytical method (FSA) was proposed by Li and his co-authors [26–29] for plates with general boundary supports. In the FSA, a fictitious Fourier cosine series was used to satisfy first the elastic BC and then the GDE to form the final eigenvalue system expressed in terms of separate stiffness and mass matrices. However, when using this method, there is no guarantee that no natural frequency of the structure will be missed and the method may become computationally expensive and very difficult in achieving high accuracies, particularly in the high frequency range. Besides, the assembly procedure in this method seems to be quite tedious and cumbersome [28,29]. The superposition method on the other hand, pioneered by Lamé [38] and extensively used by Gorman in plate vibration problems (see his review paper [39]), has been shown to be an accurate and efficient method. However, the method is not sufficiently general since different BC require different formulation, and it is limited to a single plate [30,31,40,41] or simple plate assemblies [42,43]. Nevertheless, it should be pointed out that the superposition method is an excellent idea which has partly motivated the formulation of the current S-DSM. Accurate and efficient attributes of the superposition method are preserved as well as further improvements are made in the current S-DSM with the help of the enhanced WW algorithm. Furthermore, the current S-DSM can be applied to arbitrarily prescribed boundary conditions, which was not so easily possible in the superposition method.

The research described in this paper has no-doubt opened up novel possibilities for solving complex plate and shell vibration and buckling problems in an exact and efficient manner. In Part II of this two-part paper, an extensive numerical results computation exercise is conducted to demonstrate the superiority of the proposed method in terms of its exactness, efficiency and

robustness over the conventional FEM and other analytical and semi-analytical methods.

2. Governing differential equation, general solution and boundary condition

2.1. Governing differential equation

Consider a rectangular orthotropic composite Kirchhoff plate as shown in Fig. 1 occupying the region $\Omega \times [-h/2, h/2]$, where $\Omega = [-a, a] \times [-b, b]$ denotes the midplane surface of the plate, and h is the total thickness. The composite plate consists of N_l number of specially orthotropic layers that are symmetrically aligned within Ω. If classical lamination theory [44] is applied, clearly the bending and extensional deformations will be decoupled for any symmetric laminate (in laminate notation: $B_{ij} = 0$). In this paper, attention is focused only on the transverse vibration of the plate. Using the classical Kirchhoff theory, the displacement fields of the plate can be expressed as: $u(x, y, z, t) = -z\partial w/\partial x$, $v(x, y, z, t) = -z\partial w/\partial y$ and $w(x, y, z, t) = w$. The governing differential equation (GDE) and the natural boundary conditions (BC) for the plate can be derived using Hamilton's principle [44]. For symmetric and balanced cross ply laminates, $D_{16} = D_{26} = 0$, therefore the GDE takes the form [44]

$$D_{11}\frac{\partial^4 w}{\partial x^4} + 2(D_{12} + 2D_{66})\frac{\partial^4 w}{\partial x^2 \partial y^2} + D_{22}\frac{\partial^4 w}{\partial y^4} + I_0\frac{\partial^2 w}{\partial t^2} - I_2\left(\frac{\partial^4 w}{\partial x^2 \partial t^2} + \frac{\partial^4 w}{\partial y^2 \partial t^2}\right) = 0, \tag{1}$$

where the bending stiffnesses D_{ij} of the plate and the inertia parameters I_0 and I_2 are given by

$$D_{ij} = \frac{1}{3}\sum_{k=1}^{N_l} \overline{C}_{ij}^{(k)}(z_k^3 - z_{k-1}^3), [I_0, I_2] = \sum_{k=1}^{N_l} \rho^{(k)}\left[(z_k - z_{k-1}),\ \frac{1}{3}(z_k^3 - z_{k-1}^3)\right] \tag{2}$$

and where $\rho^{(k)}$ is the mass density, $\overline{C}_{ij}^{(k)}$ is the material property matrix related to constitutive laws in the laminate coordinate system of the kth layer (see e.g., Ref. [44]).

If harmonic oscillation assumption $w(x, y, t) = W(x, y)e^{i\omega t}$ is made and the following notations are introduced

$$\Gamma = \frac{D_{12} + 2D_{66}}{D_{11}}, \quad \Lambda = \frac{D_{22}}{D_{11}}, \quad \kappa = \frac{I_0\omega^2}{D_{11}}, \quad \chi = \frac{I_2\omega^2}{D_{11}}, \tag{3}$$

the GDE of Eq. (1) can then be transformed into the frequency domain as follows

$$\frac{\partial^4 W}{\partial x^4} + 2\Gamma\frac{\partial^4 W}{\partial x^2 \partial y^2} + \Lambda\frac{\partial^4 W}{\partial y^4} + \chi\left(\frac{\partial^2 W}{\partial x^2} + \frac{\partial^2 W}{\partial y^2}\right) - \kappa W = 0. \tag{4}$$

Also, Hamilton's principle facilitates the generation of the natural boundary conditions (BC) as a by-product. Following the sign convention illustrated in Fig. 1, the natural BC along the boundaries $x = \pm a$ may be expressed as

$$\delta W: \qquad V_x = -D_{11}\left(\frac{\partial^3 W}{\partial x^3} + \Gamma^*\frac{\partial^3 W}{\partial x \partial y^2} + \chi\frac{\partial W}{\partial x}\right), \tag{5a}$$

$$\delta\phi_x = -\delta\frac{\partial W}{\partial x}: \qquad M_{xx} = -D_{11}\left(\frac{\partial^2 W}{\partial x^2} + \nu_{21}\frac{\partial^2 W}{\partial y^2}\right), \tag{5b}$$

where $\Gamma^* = 2\Gamma - \nu_{21}$. Similarly, the natural BC along $y = \pm b$ become

$$\delta W: \qquad V_y = -D_{11}\left(\Lambda\frac{\partial^3 W}{\partial y^3} + \Gamma^*\frac{\partial^3 W}{\partial y \partial x^2} + \chi\frac{\partial W}{\partial y}\right), \tag{6a}$$

$$\delta\phi_y = -\delta\frac{\partial W}{\partial y}: \qquad M_{yy} = -D_{11}\left(\Lambda\frac{\partial^2 W}{\partial y^2} + \nu_{21}\frac{\partial^2 W}{\partial x^2}\right). \tag{6b}$$

The notations ϕ_x in Eq. (5b) and ϕ_y in Eq. (6b) denote the rotations of the transverse normal about the y- and x-axes respectively (see for example p.132 in Ref. [44]). The next step will be to seek a general solution of Eq. (4).

2.2. General solution

In this section, a general solution of Eq. (4) in an exact sense is derived by superposing two sets of series solutions using the concept of the spectral method (SM) [16,17]. If the general solution is expressed as $W(x, y) = X(x)Y(y)$ on the basis of the separation of variables principle, then each series solution is derived from first representing either $X(x)$ or $Y(y)$ in terms of modified Fourier series and then solving for the other direction (either $Y(y)$ or $X(x)$).

The task of seeking the general solution for Eq. (4) is difficult unless one embarks on a Levy-type assumption. This is because the general solution not only must be capable of representing any arbitrary displacement field $W(x, y)$ which satisfies the GDE of Eq. (4) in the domain Ω, but also it must provide the flexibility to describe any arbitrary boundary conditions on the four plate boundaries. Owing to the homogeneity and the linearity, the general solution of Eq. (4) can be sought by using the method of separation of variables:

$$W(x, y) = X(x)Y(y) = Ce^{qx+py}, \tag{7}$$

where C is an arbitrary constant; q and p are the two *wave parameters* corresponding to x and y. Substituting Eq. (7) into Eq. (4) leads to the following characteristic equation

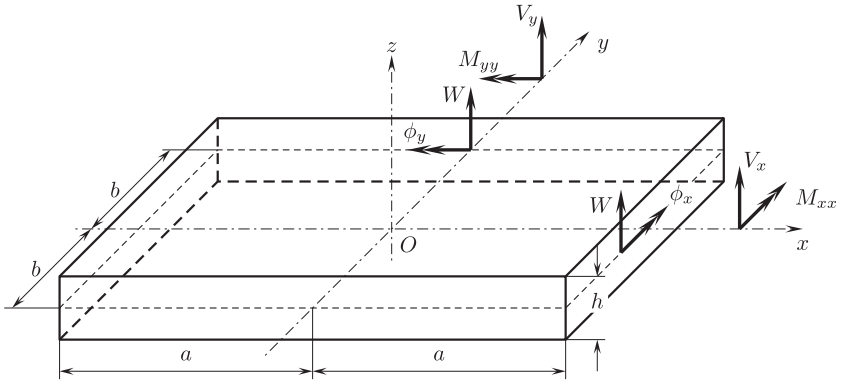

Fig. 1. Coordinate system and notations for displacements and forces for a thin laminated plate.

$$q^4 + 2\Gamma p^2 q^2 + \Lambda p^4 + \chi(q^2 + p^2) - \kappa = 0, \tag{8}$$

which gives the dispersion (spectrum) relation relating the *frequency parameter* κ and the two *wave parameters* q and p. Therefore, any combination of the wave parameters p, q and frequency parameter κ fulfilling Eq. (8) represents a solution to the GDE of Eq. (4). So there are infinite number of possibilities of such combinations. Naturally, this becomes a formidable problem giving rise to difficulties when obtaining the general solution. This is of course, very different from Levy-type solutions (e.g., see Refs. [10,11,15]) in which the pair of simply-supported opposite edges enable one to fix the wave parameter in one direction and the other wave parameter can then be expressed easily, just like the 1D beam problem (e.g., see Refs. [4–8]). The general solution for the current S-DSM is, however, resolved using the spectral method. In what follows a detailed description of the procedure is given.

Based on the concept of spectral method, any arbitrary 1D function $X(x)$ and $Y(y)$ defined in $x \in [-a, a]$ and $y \in [-b, b]$ can be represented by the modified Fourier series given in Eq. (A.1) of Appendix A as

$$X(x) = \sum_{\substack{m\in\mathbb{N}\\ k\in\{0,1\}}} \widetilde{C}_{km}\mathcal{T}_k(\alpha_{km}x), \qquad Y(y) = \sum_{\substack{n\in\mathbb{N}\\ j\in\{0,1\}}} \widetilde{C}_{jn}\mathcal{T}_j(\beta_{jn}y), \tag{9}$$

where $\mathbb{N} = \{0, 1, 2, 3, \ldots\}$, $\widetilde{C}_{km}$ and $\widetilde{C}_{jn}$ are unknown coefficients and $\mathcal{T}_k$, $\mathcal{T}_j$ denote complete orthogonal sets of Fourier basis functions with the wavenumbers α_{km} and β_{jn} taking the form

$$\alpha_{km} = \begin{cases} m\pi/a & k = 0 \\ (m + 1/2)\pi/a & k = 1 \end{cases}, \quad \beta_{jn} = \begin{cases} n\pi/b & j = 0 \\ (n + 1/2)\pi/b & j = 1 \end{cases} \tag{10}$$

where $m,\ n \in \mathbb{N}$. This is a crucial step to be undertaken to obtain the general solution. The adopted basis functions form an orthogonal complete set, in which the wavenumbers α_{km} or β_{jn} have been carefully chosen, see Eq. (10). Essentially such a series is composed of cosine and sine series. The cosine series forms a complete set to describe the symmetric component of $X(x)$ or $Y(y)$ whereas the sine series represents the anti-symmetric component. The details are referred to in Appendix A. Then for each wavenumber in one direction (α_{km} or β_{jn}), one can always obtain the analytical solution in the other direction based on the GDE. To this end, adding up the above two infinite series and also based on Euler's formula, the general solution of the GDE can be written in an exact sense as

$$\begin{aligned} W(x,y) = &\sum_{\substack{m\in\mathbb{N}\\ k\in\{0,1\}}} \mathcal{T}_k(\alpha_{km}x)[C_{km1}\cosh(p_{1km}y) + C_{km2}\cosh(p_{2km}y) \\ &+ C_{km3}\sinh(p_{1km}y) + C_{km4}\sin h(p_{2km}y)] \\ &+ \sum_{\substack{n\in\mathbb{N}\\ j=\{0,1\}}} \mathcal{T}_j(\beta_{jn}y)[C_{jn1}\cosh(q_{1jn}x) + C_{jn2}\cosh(q_{2jn}x) \\ &+ C_{jn3}\sinh(q_{1jn}x) + C_{jn4}\sinh(q_{2jn}x)]. \end{aligned} \tag{11}$$

The wave parameters p_{1km}, p_{2km} and q_{1jn}, q_{2jn} are solved by substituting $q_{km} = i\alpha_{km}$ and $p_{jn} = i\beta_{jn}$ into the characteristic Eq. (8) to obtain

$$\begin{cases} p_{1km} = \frac{1}{\sqrt{\Lambda}}\sqrt{\Gamma\alpha_{km}^2 - \frac{\chi}{2} - \sqrt{\frac{\chi^2}{4} + \chi(\Lambda - \Gamma)\alpha_{km}^2 + (\Gamma^2 - \Lambda)\alpha_{km}^4 + \Lambda\kappa}} \\ p_{2km} = \frac{1}{\sqrt{\Lambda}}\sqrt{\Gamma\alpha_{km}^2 - \frac{\chi}{2} + \sqrt{\frac{\chi^2}{4} + \chi(\Lambda - \Gamma)\alpha_{km}^2 + (\Gamma^2 - \Lambda)\alpha_{km}^4 + \Lambda\kappa}} \end{cases} \tag{12}$$

and

$$\begin{cases} q_{1jn} = \sqrt{\Gamma\beta_{jn}^2 - \frac{\chi}{2} - \sqrt{\frac{\chi^2}{4} + \chi(1 - \Gamma)\beta_{jn}^2 + (\Gamma^2 - \Lambda)\beta_{jn}^4 + \kappa}} \\ q_{2jn} = \sqrt{\Gamma\beta_{jn}^2 - \frac{\chi}{2} + \sqrt{\frac{\chi^2}{4} + \chi(1 - \Gamma)\beta_{jn}^2 + (\Gamma^2 - \Lambda)\beta_{jn}^4 + \kappa}} \end{cases}. \tag{13}$$

It can be proved [16] that the general solution of Eq. (11) establishes a complete solution space of Eq. (4). That is to say, the general solution of Eq. (11) not only satisfies the GDE of Eq. (4) rigorously, but also provides complete flexibility to describe any arbitrary boundary conditions on the four sides of the plate. As pointed out by Doyle [45], the spectral idea always establishes a close relationship between the structural dynamics and wave propagation problems. Here, the physical meaning of this general solution becomes self-explanatory if one looks from a wave propagating point of view. For example, with a given $q = i\alpha_{km}$, namely, when the plate is assumed to move harmonically with the wavenumber α_{km} in the x direction, there will be a pair of incident and reflected waves in the y direction with wave parameters p_{1km} and p_{2km}, respectively, and vice versa.

An inspection on Eq. (11) indicates that the general solution of Eq. (11) can be partitioned into a sum of four component solutions in each of which the function $W^{kj}(x,y)$ is either even or odd. Thus letting

$$W(x,y) = \sum_{k,j\in\{0,1\}} W^{kj}(x,y) = W^{00} + W^{01} + W^{10} + W^{11}, \tag{14}$$

where the indices k (related to x direction) and j (related to y direction), taking in turn with values either '0' or '1', represent either symmetric or antisymmetric functions in the related directions. Therefore, the general solution $W(x,y)$ defined in the region $\Omega = [-a, a] \times [-b, b]$ is represented by the four solution components $W^{kj}(x,y)$ defined on the first quadrant of the midplane $\Omega_1 = [0, a] \times [0, b]$ based on their symmetric or antisymmetric properties, e.g., $W^{kj}(-x,y) = (-1)^k W^{kj}(x,y)$ and $W^{kj}(x,-y) = (-1)^j W^{kj}(x,y)$. According to Eq. (11), the four solution components take the following unified form

$$\begin{aligned} W^{kj}(x,y) = &\sum_{m\in\mathbb{N}} \left[A_{1km}\mathcal{H}_j(p_{1km}y) + A_{2km}\mathcal{H}_j(p_{2km}y)\right]\mathcal{T}_k(\alpha_{km}x) \\ &+ \sum_{n\in\mathbb{N}} \left[B_{1jn}\mathcal{H}_k(q_{1jn}x) + B_{2jn}\mathcal{H}_k(q_{2jn}x)\right]\mathcal{T}_j(\beta_{jn}y), \end{aligned} \tag{15}$$

where A_{1km}, A_{2km}, B_{1jn} and B_{2jn} are unknown coefficients to be determined; $\mathcal{T}$ stands for trigonometric functions defined in Eq. (A.1) and $\mathcal{H}$ represents hyperbolic functions with the following definitions

$$\mathcal{H}_j(p_{ikm}y) = \begin{cases} \cosh(p_{ikm}y) & k = 0 \\ \sinh(p_{ikm}y) & k = 1 \end{cases}, \quad \mathcal{H}_k(q_{ijn}x) = \begin{cases} \cosh(q_{ijn}x) & j = 0 \\ \sinh(q_{ijn}x) & j = 1 \end{cases} \tag{16}$$

where $i = 1,\ 2$. Both $\mathcal{H}_j(p_{ikm}y)$ and $\mathcal{H}_k(q_{ijn}x)$ can be denoted by the unified notation below

$$\mathcal{H}_l(\Xi\xi) = \begin{cases} \mathcal{H}_j(p_{ikm}y) \text{ with } l = j, & \Xi = p_{1km} \text{ or } p_{2km}, & \xi = y \\ \mathcal{H}_k(q_{ijn}x) \text{ with } l = k, & \Xi = q_{1jn} \text{ or } q_{2jn}, & \xi = x \end{cases}. \tag{17}$$

Some useful properties of the above trigonometric $\mathcal{T}$ and hyperbolic $\mathcal{H}$ functions will be introduced later. By using the notation

$$\mathcal{H}_l^*(\Xi\xi) = \frac{\mathrm{d}\mathcal{H}_l(\Xi\xi)}{\Xi\mathrm{d}\xi}, \tag{18}$$

the following relationships can be obtained based on the properties of hyperbolic function

$$\frac{\mathrm{d}^i\mathcal{H}_l(\Xi\xi)}{\mathrm{d}\xi^i} = \begin{cases} \Xi^i\mathcal{H}_l(\Xi\xi), & i \text{ is even} \\ \Xi^i\mathcal{H}_l^*(\Xi\xi), & i \text{ is odd} \end{cases}. \tag{19}$$

The properties of trigonometric function $\mathcal{T}$ based on differentiation rules is given in Eq. (A.2). Also, a careful inspection on Eqs. (12) and

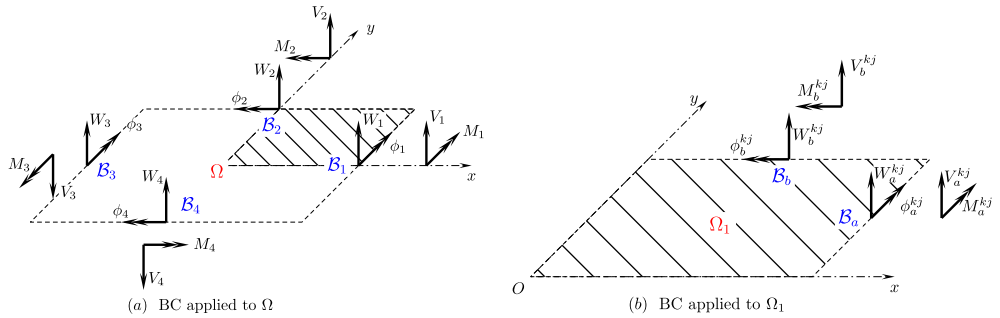

Fig. 2. Illustration of the arbitrarily prescribed boundary conditions applied on the entire plate Ω in (a) which are partitioned into four kj BC components which are prescribed to the quarter plate as in (b).

(13) gives the following identities which will be used in later formulations.

$$p_{1km}^2 + p_{2km}^2 = (2\Gamma\alpha_{km}^2 - \chi)/\Lambda, \quad p_{1km}^2 p_{2km}^2 = (\alpha_{km}^4 - \chi\alpha_{km}^2 - \kappa)/\Lambda, \tag{20a}$$

$$q_{1jn}^2 + q_{2jn}^2 = 2\Gamma\beta_{jn}^2 - \chi, \quad q_{1jn}^2 q_{2jn}^2 = \Lambda\beta_{jn}^4 - \chi\beta_{jn}^2 - \kappa, \tag{20b}$$

$$\Lambda(p_{1km}^2 + \beta_{jn}^2)(p_{2km}^2 + \beta_{jn}^2) = (q_{1jn}^2 + \alpha_{km}^2)(q_{2jn}^2 + \alpha_{km}^2). \tag{20c}$$

2.3. Boundary conditions

Previously, the general solution $W(x,y)$ which is defined in the domain Ω (Fig. 2(a)) has been partitioned into four components $W^{kj}(x,y)$ defined within Ω_1 (first quarter of Ω, see Fig. 2(b)) with different symmetric/antisymmetric properties, with kj taking four different combinations of '0' and '1'. In this section, the arbitrarily prescribed BC prescribed along the four boundaries $\mathcal{B}_1 \sim \mathcal{B}_4$ (Fig. 2(a)) will be partitioned into four corresponding BC components imposed on the two boundaries $\mathcal{B}_a$ and $\mathcal{B}_b$ of the plate quarter Ω_1, see Fig. 2(b).

Without loss of generality, any arbitrarily prescribed displacement and force BC on the four plate edges of Ω can be written in vector form as

$$\begin{bmatrix} W_1 \\ \phi_1 \\ W_2 \\ \phi_2 \\ W_3 \\ \phi_3 \\ W_4 \\ \phi_4 \end{bmatrix} = \begin{bmatrix} W(a,y) \\ \phi_x(a,y) \\ W(x,b) \\ \phi_y(x,b) \\ W(-a,y) \\ \phi_x(-a,y) \\ W(x,-b) \\ \phi_y(x,-b) \end{bmatrix}, \quad \begin{bmatrix} V_1 \\ M_1 \\ V_2 \\ M_2 \\ V_3 \\ M_3 \\ V_4 \\ M_4 \end{bmatrix} = \begin{bmatrix} V_x(a,y) \\ M_{xx}(a,y) \\ V_y(x,b) \\ M_{yy}(x,b) \\ -V_x(-a,y) \\ -M_{xx}(-a,y) \\ -V_y(x,-b) \\ -M_{yy}(x,-b) \end{bmatrix}, \tag{21}$$

where W_i, ϕ_i, V_i and M_i are introduced for the BC prescribed along boundary $\mathcal{B}_i$ ($i = 1, 2, 3, 4$ as shown in Fig. 2(a)).

On substituting general solution of Eq. (14) into the general BC of Eqs. (5) and (6), both the general force and displacement BC can be decomposed into four kj components as below.

$$\begin{bmatrix} W_a^{kj} \\ W_b^{kj} \\ \phi_a^{kj} \\ \phi_b^{kj} \end{bmatrix} = \begin{bmatrix} W^{kj}|_{x=a} \\ W^{kj}|_{y=b} \\ -\partial_x W^{kj}|_{x=a} \\ -\partial_y W^{kj}|_{y=b} \end{bmatrix}, \quad \begin{bmatrix} V_a^{kj} \\ V_b^{kj} \\ M_a^{kj} \\ M_b^{kj} \end{bmatrix} = D_{11} \begin{bmatrix} -\left(\partial_x^3 + \Gamma^*\partial_x\partial_y^2 + \chi\partial_x\right) W^{kj}|_{x=a} \\ -\left(\Lambda\partial_y^3 + \Gamma^*\partial_y\partial_x^2 + \chi\partial_y\right) W^{kj}|_{y=b} \\ -\left(\partial_x^2 + \nu_{21}\partial_y^2\right) W^{kj}|_{x=a} \\ -\left(\Lambda\partial_y^2 + \nu_{21}\partial_x^2\right) W^{kj}|_{y=b} \end{bmatrix}, \tag{22}$$

where ∂_x^i and ∂_y^i denote the differential operators $\partial_x^i = \partial^i/\partial x^i$ and $\partial_y^i = \partial^i/\partial y^i$. In Eq. (22), the terms labelled with the subscript a or b indicate the corresponding boundary conditions applied along $\mathcal{B}_a$ and $\mathcal{B}_b$ of the quarter plate respectively, see Fig. 2(b).

Therefore, the relationships between the arbitrarily prescribed boundary conditions of Eq. (21) and its four components of Eq. (22) can be established. These are recorded in Appendix B, which will be used later in the DS development.

3. Development of the dynamic stiffness matrix

In general, the dynamic stiffness (DS) matrix of a structure is formulated by substituting the general solution into the displacement and the force BC and then eliminating the unknowns coefficients from the general solution. Although more or less the same idea applies for the current S-DSM development, there are however, still some differences when compared with that of the classical DSM development.

In the current S-DSM, both the general solution and the arbitrarily prescribed BC have been decomposed into four kj components with different symmetry/antisymmetry properties, see Eqs. (15) and (22). Therefore, one can develop the DS component matrices $\boldsymbol{K}^{kj}$ corresponding to each kj components. Subsequently, by considering the relationships between the BC of the whole plate and its four BC components as given in Eqs. (B.2) and (B.3), these four DS component matrices $\boldsymbol{K}^{kj}$ can be assembled to form effectively the DS matrix $\boldsymbol{K}$ for the entire plate for the most general case. In doing so, the formulation is symbolically simplified and thus computational cost is significantly reduced.

Moreover, due to the application of Fourier series, careful attention is to be paid during the S-DSM development to ensure that the formulated DS matrices are symmetric, so as to enable the application of the Wittrick–Williams algorithm.

Finally, the DS component matrix $\boldsymbol{K}^{kj}$ is generated through a mixed-variable formulation which makes the current method efficient, accurate and numerically stable when compared with the classical DS formulation. In the present method, the unknown coefficients in the general solution are eliminated based on some, but not all, of the boundary conditions. Then the remaining boundary conditions are applied to form a mixed-variable algebraic system which is subsequently used to formulate the DS component matrix $\boldsymbol{K}^{kj}$. By contrast, if the classical DS formulation was used, both the force $\boldsymbol{f}^{kj}$ and the displacement boundary conditions $\boldsymbol{d}^{kj}$ would have to be expressed in terms of unknown coefficient $\boldsymbol{c}^{kj}$, i.e., $\boldsymbol{d}^{kj} = \boldsymbol{D}^{kj}\boldsymbol{c}^{kj}$ and $\boldsymbol{f}^{kj} = \boldsymbol{F}^{kj}\boldsymbol{c}^{kj}$ and the DS matrix is given by $\boldsymbol{K}^{kj} = \boldsymbol{F}^{kj}\boldsymbol{D}^{kj^{-1}}$. The inverse of the matrix $\boldsymbol{D}^{kj}$ for the current case requires more computational resources and may cause numerical ill-conditioning. This might be the case especially when more terms are included in the Fourier series.

3.1. Formulation of the DS component matrix $\boldsymbol{K}^{kj}$

The formulation of $\boldsymbol{K}^{kj}$ is accomplished in three steps: (i) The BC are represented by a modified Fourier series, (ii) The unknown

coefficients A_{1km}, A_{2km}, B_{1jn} and B_{2jn} appearing in the general solution are solved based on some of the BC and (iii) Through a mixed-variable formulation procedure, the remaining BC lead to an infinite system of mixed-variable form which is finally used to arrive at the DS component matrix $\boldsymbol{K}^{kj}$. Note that in what follows the procedure is valid for all of the four symmetric/antisymmetric component cases by taking k and j in turn with values either '0' or '1'.

3.1.1. Formulation of boundary-condition components using modified Fourier series

In the last section, the BC components of Eq. (22) have been expressed by the general solution and its derivatives. Alternatively, the BC components of Eq. (22) can be represented by modified Fourier series of Eq. (A.3), which will be combined with those expressions of Eq. (22) to finally formulate the DS component matrix $\boldsymbol{K}^{kj}$.

Here the same set of Fourier basis functions of Eq. (A.1) is adopted as in Eq. (9), but appropriate Fourier series formula should be chosen to keep the symplecticity [46] of the formulated matrix system and therefore, ensuring the symmetry of the resulting DS matrix. In this method, the modified Fourier series of Eq. (A.3) in Appendix A is adopted, and hence the entries of the BC component vectors on the left-hand sides of Eq. (22) can be alternatively expressed as

$$\begin{bmatrix} W_a^{kj} \\ W_b^{kj} \\ \phi_a^{kj} \\ \phi_b^{kj} \end{bmatrix} = \begin{bmatrix} \sum_{n\in\mathbb{N}} W_{ajn} \frac{\mathcal{T}_j(\beta_{jn}y)}{\sqrt{\zeta_{jn}b}} \\ \sum_{m\in\mathbb{N}} W_{bkm} \frac{\mathcal{T}_k(\alpha_{km}x)}{\sqrt{\zeta_{km}a}} \\ \sum_{n\in\mathbb{N}} \phi_{ajn} \frac{\mathcal{T}_j(\beta_{jn}y)}{\sqrt{\zeta_{jn}b}} \\ \sum_{m\in\mathbb{N}} \phi_{bkm} \frac{\mathcal{T}_k(\alpha_{km}x)}{\sqrt{\zeta_{km}a}} \end{bmatrix}, \quad \begin{bmatrix} V_a^{kj} \\ V_b^{kj} \\ M_a^{kj} \\ M_b^{kj} \end{bmatrix} = D_{11} \begin{bmatrix} \sum_{n\in\mathbb{N}} V_{ajn} \frac{\mathcal{T}_j(\beta_{jn}y)}{\sqrt{\zeta_{jn}b}} \\ \sum_{m\in\mathbb{N}} V_{bkm} \frac{\mathcal{T}_k(\alpha_{km}x)}{\sqrt{\zeta_{km}a}} \\ \sum_{n\in\mathbb{N}} M_{ajn} \frac{\mathcal{T}_j(\beta_{jn}y)}{\sqrt{\zeta_{jn}b}} \\ \sum_{m\in\mathbb{N}} M_{bkm} \frac{\mathcal{T}_k(\alpha_{km}x)}{\sqrt{\zeta_{km}a}} \end{bmatrix} \tag{23}$$

where the superscripts kj for the Fourier coefficients such as W_{ajn} and V_{bkm} are omitted for notational convenience. The Fourier coefficients of the boundary conditions (e.g. W_{ajn} and V_{bkm}) in Eq. (23) were obtained from Eq. (A.3) to give

$$W_{ajn} = \int_{-b}^{b} W_a^{kj} \frac{\mathcal{T}_j(\beta_{jn}y)}{\sqrt{\zeta_{jn}b}} \mathrm{d}y, \quad V_{bkm} = \int_{-a}^{a} \frac{V_b^{kj}}{D_{11}} \frac{\mathcal{T}_k(\alpha_{km}x)}{\sqrt{\zeta_{km}a}} \mathrm{d}x. \tag{24}$$

The $\sqrt{\zeta_{jn}b}$ and $\sqrt{\zeta_{km}a}$ appearing in Eqs. (23), and (24) provide the symmetry of the forward and inverse Fourier transformation to eliminate the dependence of the length in the integral ranges $[-b,b]$ or $[-a,a]$. Therefore, when $a \neq b$ the ensuing DS component matrices $\boldsymbol{K}^{kj}$ will remain symmetric. This will become apparent later.

3.1.2. The determination of the unknown coefficients in the general solution

In view of Eqs. (A.2) and (19), the expressions for ϕ_a^{kj} and V_a^{kj} given in Eqs. (22) and (23) lead to

$$-\partial_x W^{kj}\big|_{x=a} = \sum_{n\in\mathbb{N}} \phi_{ajn} \mathcal{T}_j(\beta_{jn}y) \Big/ \sqrt{\zeta_{jn}b}, \tag{25a}$$

$$-(\partial_x^3 + \Gamma^*\partial_x\partial_y^2 + \chi\partial_x) W^{kj}\big|_{x=a} = \sum_{n\in\mathbb{N}} V_{ajn} \mathcal{T}_j(\beta_{jn}y) \Big/ \sqrt{\zeta_{jn}b}, \tag{25b}$$

which yield

$$-\phi_{ajn}/\sqrt{\zeta_{jn}b} = q_{1jn}\mathcal{H}_k^*(q_{1jn}a)B_{1jn} + q_{2jn}\mathcal{H}_k^*(q_{2jn}a)B_{2jn}, \tag{26a}$$

$$\begin{aligned} -V_{ajn}/\sqrt{\zeta_{jn}b} = {} & \left(q_{1jn}^2 - \Gamma^*\beta_{jn}^2 + \chi\right) q_{1jn}\mathcal{H}_k^*(q_{1jn}a)B_{1jn} \\ & + \left(q_{2jn}^2 - \Gamma^*\beta_{jn}^2 + \chi\right) q_{2jn}\mathcal{H}_k^*(q_{2jn}a)B_{2jn} \end{aligned} \tag{26b}$$

for all $n \in \mathbb{N}$. With the help of Eq. (20b), the unknowns coefficients B_{1jn} and B_{2jn} can be determined from Eq. (26) for all $n \in \mathbb{N}$ to give

$$B_{1jn} = \frac{V_{ajn} - (\nu_{21}\beta_{jn}^2 - q_{1jn}^2)\phi_{ajn}}{\sqrt{\zeta_{jn}b} q_{1jn}\mathcal{H}_k^*(q_{1jn}a)(q_{2jn}^2 - q_{1jn}^2)}, \tag{27a}$$

$$B_{2jn} = -\frac{V_{ajn} - (\nu_{21}\beta_{jn}^2 - q_{2jn}^2)\phi_{ajn}}{\sqrt{\zeta_{jn}b} q_{2jn}\mathcal{H}_k^*(q_{2jn}a)(q_{2jn}^2 - q_{1jn}^2)}. \tag{27b}$$

Similarly, with the help of Eq. (20a), the expressions of ϕ_b^{kj} and V_b^{kj} in Eqs. (22) and (23) yield the unknowns A_{1km} and A_{2km} to be

$$A_{1km} = \frac{V_{bkm} - (\nu_{21}\alpha_{km}^2 - \Lambda p_{1km}^2)\phi_{bkm}}{\sqrt{\zeta_{km}a} p_{1km}\mathcal{H}_j^*(p_{1km}b)(p_{2km}^2 - p_{1km}^2)}, \tag{28a}$$

$$A_{2km} = -\frac{V_{bkm} - (\nu_{21}\alpha_{km}^2 - \Lambda p_{2km}^2)\phi_{bkm}}{\sqrt{\zeta_{km}a} p_{2km}\mathcal{H}_j^*(p_{2km}b)(p_{2km}^2 - p_{1km}^2)}. \tag{28b}$$

3.1.3. Infinite system and the formulation of the DS component matrix $\boldsymbol{K}^{kj}$

So far, all unknown coefficients A_{1km}, A_{2km}, B_{1jn} and B_{2jn} in the solution component of Eq. (15) have been determined using the entries ϕ_a^{kj}, ϕ_b^{kj}, V_a^{kj} and V_b^{kj} in the BC components of Eqs. (22) and (23). Subsequently, an infinite system of algebraic equations is derived by substituting the above determined unknowns into the remaining entries W_a^{kj}, W_b^{kj}, M_a^{kj} and M_b^{kj} in Eqs. (22) and (23), see Appendix C for details. This infinite system can be rewritten in the following mixed-variable matrix form as:

$$\begin{bmatrix} \boldsymbol{W}^{kj} \\ \boldsymbol{M}^{kj} \end{bmatrix} = \begin{bmatrix} \boldsymbol{A}_{W\Phi}^{kj} & \boldsymbol{A}_{WV}^{kj} \\ \boldsymbol{A}_{M\Phi}^{kj} & \boldsymbol{A}_{MV}^{kj} \end{bmatrix} \begin{bmatrix} \boldsymbol{\Phi}^{kj} \\ \boldsymbol{V}^{kj} \end{bmatrix}. \tag{29}$$

The explicit expressions of the four coefficient matrices $\boldsymbol{A}^{kj}$ in Eq. (29) are given in Appendix D, with each expression denoting a clear physical meaning. The whole mixed-variable matrix in Eq. (29) exhibits a symplectic structure: $\boldsymbol{A}_{WV}^{kj} = \boldsymbol{A}_{WV}^{kj\,T}$ and $\boldsymbol{A}_{M\Phi}^{kj} = \boldsymbol{A}_{M\Phi}^{kj\,T}$ are symmetric matrices, while $\boldsymbol{A}_{W\Phi}^{kj} = -\boldsymbol{A}_{MV}^{kj\,T}$. This is because the adoption of the modified Fourier series formula (A.3) keeps the symplecticity of the Hamiltonian system. The symplecticity of this system can be proved analytically based on the minimum potential energy through the application of variational principle [46]. The sub-vectors in Eq. (29) are defined as

$$\boldsymbol{V}^{kj} = \begin{bmatrix} \boldsymbol{V}_a^{kj} \\ \boldsymbol{V}_b^{kj} \end{bmatrix}, \quad \boldsymbol{M}^{kj} = \begin{bmatrix} \boldsymbol{M}_a^{kj} \\ \boldsymbol{M}_b^{kj} \end{bmatrix}, \quad \boldsymbol{W}^{kj} = \begin{bmatrix} \boldsymbol{W}_a^{kj} \\ \boldsymbol{W}_b^{kj} \end{bmatrix}, \quad \boldsymbol{\Phi}^{kj} = \begin{bmatrix} \boldsymbol{\Phi}_a^{kj} \\ \boldsymbol{\Phi}_b^{kj} \end{bmatrix} \tag{30}$$

where

$$\begin{aligned} \boldsymbol{V}_a^{kj} &= [V_{aj0}, V_{aj1}, \ldots, V_{ajn}, \cdots]^T, & \boldsymbol{V}_b^{kj} &= [V_{bk0}, V_{bk1}, \cdots, V_{bkm}, \ldots]^T, \\ \boldsymbol{M}_a^{kj} &= [M_{aj0}, M_{aj1}, \ldots, M_{ajn}, \ldots]^T, & \boldsymbol{M}_b^{kj} &= [M_{bk0}, M_{bk1}, \ldots, M_{bkm}, \ldots]^T, \\ \boldsymbol{W}_a^{kj} &= [W_{aj0}, W_{aj1}, \ldots, W_{ajn}, \ldots]^T, & \boldsymbol{W}_b^{kj} &= [W_{bk0}, W_{bk1}, \ldots, W_{bkm}, \ldots]^T, \\ \boldsymbol{\Phi}_a^{kj} &= [\phi_{aj0}, \phi_{aj1}, \ldots, \phi_{ajn}, \ldots]^T, & \boldsymbol{\Phi}_b^{kj} &= [\phi_{bk0}, \phi_{bk1}, \ldots, \phi_{bkm}, \cdots]^T \end{aligned}$$

are the vectors whose entries are the Fourier coefficients in Eq. (23). Each entry of the above vectors corresponds to a frequency–wavenumber dependent DOF. Two particular boundary conditions need special mention. When the plate is completely free on all of its four edges, one has $\boldsymbol{M}^{kj} = \boldsymbol{V}^{kj} = \boldsymbol{0}$, the system of Eq. (29) is reduced to the homogeneous system $\boldsymbol{A}_{M\Phi}^{kj}\boldsymbol{\Phi}^{kj} = \boldsymbol{0}$; whereas when the plate is fully clamped all around its edges with $\boldsymbol{W}^{kj} = \boldsymbol{\Phi}^{kj} = \boldsymbol{0}$, the system of Eq. (29) becomes $\boldsymbol{A}_{WV}^{kj}\boldsymbol{V}^{kj} = \boldsymbol{0}$. Therefore, the natural frequencies in these two special cases can be computed by applying the Wittrick–Williams algorithm directly to $\boldsymbol{A}_{M\Phi}^{kj}$ and $\boldsymbol{A}_{WV}^{kj}$ respectively.

On the basis of Eq. (29), the DS matrix for each kj component can be reconstructed in the following form

$$\boldsymbol{f}^{kj} = \boldsymbol{K}^{kj}\boldsymbol{d}^{kj}, \tag{31}$$

where

$$\boldsymbol{f}^{kj} = D_{11}\begin{bmatrix}\boldsymbol{V}^{kj}\\ \boldsymbol{M}^{kj}\end{bmatrix}, \quad \boldsymbol{d}^{kj} = \begin{bmatrix}\boldsymbol{W}^{kj}\\ \boldsymbol{\Phi}^{kj}\end{bmatrix},$$

$$\boldsymbol{K}^{kj} = D_{11}\begin{bmatrix}\boldsymbol{A}_{WV}^{kj\ -1} & -\boldsymbol{A}_{WV}^{kj\ -1}\boldsymbol{A}_{W\Phi}^{kj}\\ \boldsymbol{A}_{MV}^{kj}\boldsymbol{A}_{WV}^{kj\ -1} & \boldsymbol{A}_{M\Phi}^{kj} - \boldsymbol{A}_{MV}^{kj}\boldsymbol{A}_{WV}^{kj\ -1}\boldsymbol{A}_{W\Phi}^{kj}\end{bmatrix}.$$

3.2. Using the DS component matrix $\boldsymbol{K}^{kj}$ to form the DS matrix $\boldsymbol{K}$ for the entire plate element

In this section, the previous DS component matrices $\boldsymbol{K}^{kj}$ defined in the domain Ω_1 of the quarter plate are assembled to form the DS matrix $\boldsymbol{K}$ in the domain Ω of the entire plate. This is achieved by considering the relationships of the BC for the quarter plate and the entire plate (see Eqs. (B.2) and (B.3)).

As in Eq. (31), $\boldsymbol{f}^{kj}$ and $\boldsymbol{d}^{kj}$ are the Fourier coefficient vectors of the BC on $\mathcal{B}_a$, $\mathcal{B}_b$ of the quarter plate (see Fig. 2(b)) through the use of modified Fourier series of Eq. (A.3). Similarly, by applying Eq. (A.3) to the force and displacement BC of the entire plate (see Eq. (21)), one has the corresponding Fourier coefficient vectors

$$\boldsymbol{f} = [\boldsymbol{f}_1, \boldsymbol{f}_2, \boldsymbol{f}_3, \boldsymbol{f}_4]^T, \quad \boldsymbol{d} = [\boldsymbol{d}_1, \boldsymbol{d}_2, \boldsymbol{d}_3, \boldsymbol{d}_4]^T, \tag{32}$$

in which

$$\boldsymbol{f}_i = \left[\boldsymbol{V}_i^0, \boldsymbol{V}_i^1, \boldsymbol{M}_i^0, \boldsymbol{M}_i^1\right]^T, \quad \boldsymbol{d}_i = \left[\boldsymbol{W}_i^0, \boldsymbol{W}_i^1, \boldsymbol{\Phi}_i^0, \boldsymbol{\Phi}_i^1\right]^T \tag{33}$$

and where the sub-vectors such as $\boldsymbol{V}_i^1$ and $\boldsymbol{W}_i^0$ are essentially the Fourier coefficient vectors of the BC on $\mathcal{B}_i$ of the entire plate given in Eq. (21), see Fig. 2. The superscripts, being '0' or '1', stand for the Fourier cosine or sine transform of the corresponding BC on boundary $\mathcal{B}_i$. It should be kept in mind that every element of $\boldsymbol{f}$ or $\boldsymbol{d}$ corresponds to a frequency–wavenumber dependent DOF (FWDOF) on one boundary of the entire plate.

Now the relationships between $\boldsymbol{f}$, $\boldsymbol{d}$ and $\boldsymbol{f}^{kj}$, $\boldsymbol{d}^{kj}$ can be established by considering the relationships given by Eqs. (B.2) and (B.3). Introducing the transfer matrix $\boldsymbol{T}$ so that

$$\boldsymbol{f} = \boldsymbol{T}[\boldsymbol{f}^{00}, \boldsymbol{f}^{01}, \boldsymbol{f}^{10}, \boldsymbol{f}^{11}]^T, \quad \boldsymbol{d} = \boldsymbol{T}[\boldsymbol{d}^{00}, \boldsymbol{d}^{01}, \boldsymbol{d}^{10}, \boldsymbol{d}^{11}]^T. \tag{34}$$

$\boldsymbol{T}$ is the transfer matrix in the form

$$\boldsymbol{T} = \begin{bmatrix}
\boldsymbol{I}_n & \boldsymbol{O} & \boldsymbol{O} & \boldsymbol{O} & \boldsymbol{O} & \boldsymbol{O} & \boldsymbol{O} & \boldsymbol{I}_n & \boldsymbol{O} & \boldsymbol{O} & \boldsymbol{O} & \boldsymbol{O} & \boldsymbol{O} & \boldsymbol{O} & \boldsymbol{O}\\
\boldsymbol{O} & \boldsymbol{O} & \boldsymbol{O} & \boldsymbol{O} & \boldsymbol{I}_n & \boldsymbol{O} & \boldsymbol{O} & \boldsymbol{O} & \boldsymbol{O} & \boldsymbol{O} & \boldsymbol{O} & \boldsymbol{I}_n & \boldsymbol{O} & \boldsymbol{O} & \boldsymbol{O}\\
\boldsymbol{O} & \boldsymbol{I}_n & \boldsymbol{O} & \boldsymbol{O} & \boldsymbol{O} & \boldsymbol{O} & \boldsymbol{O} & \boldsymbol{O} & \boldsymbol{I}_n & \boldsymbol{O} & \boldsymbol{O} & \boldsymbol{O} & \boldsymbol{O} & \boldsymbol{O} & \boldsymbol{O}\\
\boldsymbol{O} & \boldsymbol{O} & \boldsymbol{O} & \boldsymbol{O} & \boldsymbol{O} & \boldsymbol{I}_n & \boldsymbol{O} & \boldsymbol{O} & \boldsymbol{O} & \boldsymbol{O} & \boldsymbol{O} & \boldsymbol{O} & \boldsymbol{I}_n & \boldsymbol{O} & \boldsymbol{O}\\
\boldsymbol{O} & \boldsymbol{O} & \boldsymbol{I}_m & \boldsymbol{O} & \boldsymbol{O} & \boldsymbol{O} & \boldsymbol{I}_m & \boldsymbol{O} & \boldsymbol{O} & \boldsymbol{O} & \boldsymbol{O} & \boldsymbol{O} & \boldsymbol{O} & \boldsymbol{O} & \boldsymbol{O}\\
\boldsymbol{O} & \boldsymbol{O} & \boldsymbol{O} & \boldsymbol{O} & \boldsymbol{O} & \boldsymbol{O} & \boldsymbol{O} & \boldsymbol{O} & \boldsymbol{O} & \boldsymbol{O} & \boldsymbol{I}_m & \boldsymbol{O} & \boldsymbol{O} & \boldsymbol{O} & \boldsymbol{I}_m & \boldsymbol{O}\\
\boldsymbol{O} & \boldsymbol{O} & \boldsymbol{O} & \boldsymbol{I}_m & \boldsymbol{O} & \boldsymbol{O} & \boldsymbol{O} & \boldsymbol{I}_m & \boldsymbol{O} & \boldsymbol{O} & \boldsymbol{O} & \boldsymbol{O} & \boldsymbol{O} & \boldsymbol{O} & \boldsymbol{O} & \boldsymbol{O}\\
\boldsymbol{O} & \boldsymbol{O} & \boldsymbol{O} & \boldsymbol{O} & \boldsymbol{O} & \boldsymbol{O} & \boldsymbol{O} & \boldsymbol{O} & \boldsymbol{O} & \boldsymbol{O} & \boldsymbol{O} & \boldsymbol{I}_m & \boldsymbol{O} & \boldsymbol{O} & \boldsymbol{O} & \boldsymbol{I}_m\\
-\boldsymbol{I}_n & \boldsymbol{O} & \boldsymbol{O} & \boldsymbol{O} & \boldsymbol{O} & \boldsymbol{O} & \boldsymbol{O} & \boldsymbol{O} & \boldsymbol{I}_n & \boldsymbol{O} & \boldsymbol{O} & \boldsymbol{O} & \boldsymbol{O} & \boldsymbol{O} & \boldsymbol{O} & \boldsymbol{O}\\
\boldsymbol{O} & \boldsymbol{O} & \boldsymbol{O} & \boldsymbol{O} & -\boldsymbol{I}_n & \boldsymbol{O} & \boldsymbol{O} & \boldsymbol{O} & \boldsymbol{O} & \boldsymbol{O} & \boldsymbol{O} & \boldsymbol{O} & \boldsymbol{I}_n & \boldsymbol{O} & \boldsymbol{O} & \boldsymbol{O}\\
\boldsymbol{O} & \boldsymbol{I}_n & \boldsymbol{O} & \boldsymbol{O} & \boldsymbol{O} & \boldsymbol{O} & \boldsymbol{O} & \boldsymbol{O} & \boldsymbol{O} & -\boldsymbol{I}_n & \boldsymbol{O} & \boldsymbol{O} & \boldsymbol{O} & \boldsymbol{O} & \boldsymbol{O} & \boldsymbol{O}\\
\boldsymbol{O} & \boldsymbol{O} & \boldsymbol{O} & \boldsymbol{O} & \boldsymbol{I}_n & \boldsymbol{O} & \boldsymbol{O} & \boldsymbol{O} & \boldsymbol{O} & \boldsymbol{O} & \boldsymbol{O} & \boldsymbol{O} & -\boldsymbol{I}_n & \boldsymbol{O} & \boldsymbol{O} & \boldsymbol{O}\\
\boldsymbol{O} & \boldsymbol{O} & -\boldsymbol{I}_m & \boldsymbol{O} & \boldsymbol{O} & \boldsymbol{O} & \boldsymbol{I}_m & \boldsymbol{O} & \boldsymbol{O} & \boldsymbol{O} & \boldsymbol{O} & \boldsymbol{O} & \boldsymbol{O} & \boldsymbol{O} & \boldsymbol{O} & \boldsymbol{O}\\
\boldsymbol{O} & \boldsymbol{O} & \boldsymbol{O} & \boldsymbol{O} & \boldsymbol{O} & \boldsymbol{O} & \boldsymbol{O} & \boldsymbol{O} & \boldsymbol{O} & \boldsymbol{O} & -\boldsymbol{I}_m & \boldsymbol{O} & \boldsymbol{O} & \boldsymbol{O} & \boldsymbol{I}_m & \boldsymbol{O}\\
\boldsymbol{O} & \boldsymbol{O} & \boldsymbol{O} & \boldsymbol{I}_m & \boldsymbol{O} & \boldsymbol{O} & \boldsymbol{O} & -\boldsymbol{I}_m & \boldsymbol{O} & \boldsymbol{O} & \boldsymbol{O} & \boldsymbol{O} & \boldsymbol{O} & \boldsymbol{O} & \boldsymbol{O} & \boldsymbol{O}\\
\boldsymbol{O} & \boldsymbol{O} & \boldsymbol{O} & \boldsymbol{O} & \boldsymbol{O} & \boldsymbol{O} & \boldsymbol{O} & \boldsymbol{O} & \boldsymbol{O} & \boldsymbol{O} & \boldsymbol{I}_m & \boldsymbol{O} & \boldsymbol{O} & \boldsymbol{O} & -\boldsymbol{I}_m
\end{bmatrix}, \tag{35}$$

where $\boldsymbol{I}_n$ and $\boldsymbol{I}_m$ are identity matrices of dimension n and m respectively, and $\boldsymbol{O}$ represents null matrices. It is easily seen that $\boldsymbol{T}$ is the combination of certain number of $\boldsymbol{T}_\tau$ as indicated in Eq. (B.3) (the number depends on the number of terms included in the Fourier series). As expected, $\boldsymbol{T}$ has the inherent property which is dependent on $\boldsymbol{T}_\tau$, see Eq. (B.5), and consequently

$$\boldsymbol{T}^{-1} = \boldsymbol{T}^T/2, \quad \forall\ M,\ N \in \mathbb{N}. \tag{36}$$

Now returning to Eq. (34) one has

$$\left[\boldsymbol{d}^{00}, \boldsymbol{d}^{01}, \boldsymbol{d}^{10}, \boldsymbol{d}^{11}\right]^T = \frac{1}{2}\boldsymbol{T}^T\boldsymbol{d}. \tag{37}$$

Finally, putting Eqs. (31), (32), (34) and (37) together yields the DS matrix for the entire plate element as

$$\boldsymbol{f} = \boldsymbol{K}\boldsymbol{d}, \tag{38}$$

where

$$\boldsymbol{K} = \frac{1}{2}\boldsymbol{T}\begin{bmatrix}\boldsymbol{K}^{00} & \boldsymbol{O} & \boldsymbol{O} & \boldsymbol{O}\\ \boldsymbol{O} & \boldsymbol{K}^{01} & \boldsymbol{O} & \boldsymbol{O}\\ \boldsymbol{O} & \boldsymbol{O} & \boldsymbol{K}^{10} & \boldsymbol{O}\\ \boldsymbol{O} & \boldsymbol{O} & \boldsymbol{O} & \boldsymbol{K}^{11}\end{bmatrix}\boldsymbol{T}^T \tag{39}$$

is the DS matrix of the entire plate element, which relates the Fourier coefficient vectors of the force $\boldsymbol{f}$ to that of the displacement $\boldsymbol{d}$ on the four edges of the plate.

Note that so far all of the above formulation are exact since $m,\ n \in [0, \infty)$. However, for computational purposes, the infinite series/matrices need to be truncated at certain point. It is worth highlighting that the size of the matrix in the current S-DSM is significantly smaller than that of the conventional finite element (FEM) or boundary element methods (BEM). This is mainly due to two reasons. On the one hand, the small size of the DS matrix arises from the *boundary* formulation, because the DS matrix relates the forces and displacements along the plate *boundaries* in stead of in the plate *domain*. In this respect, the S-DSM shows resemblance with the BEM. With $m \in [0, M-1]$ and $n \in [0, N-1]$ respectively, the order of the matrices are: $(M+N)\times(M+N)$ for $\boldsymbol{A}^{kj}$, $2(M+N)\times 2(M+N)$ for $\boldsymbol{K}^{kj}$ and $8(M+N)\times 8(M+N)$ for $\boldsymbol{K}$. That is to say, the order of the matrices are linear with the *sum* of M and N (the numbers of FWDOF in x and y coordinates) instead of being proportional to the *product* of M and N as in the case of FEM for a $M\times N$ mesh. On the other hand, since the current S-DSM falls into the *spectral* (both time- and spatial-wise) decomposition strategy rather than spatial discretisation like the FEM and BEM, it is self-evident that much fewer FWDOF are required in S-DSM, and yet an exact or almost exact description of the deformation field can be achieved. Naturally the size of present DS matrix is significantly smaller owing to its spectral properties.

4. Assembly procedure and the application of arbitrarily prescribed boundary conditions

In this section, the dynamic stiffness (DS) matrices $\boldsymbol{K}$ developed above for individual plate elements are assembled to form the overall DS matrix $\boldsymbol{K}_f$ of the final structure. A single element can, of course, be considered as the final structure as a special case. The application procedure of any prescribed boundary conditions for the final structure (i.e., $\boldsymbol{f}_f$ and $\boldsymbol{d}_f$) is also discussed in this section.

4.1. Assembly procedure

Like the classical DSM formulation, the assembly procedure for the current S-DSM also resembles closely the finite element method (FEM) with the exception that each plate element is connected through line nodes instead of point nodes. There are

however, some differences in the assembly procedure between the current method and the classical DSM using a Levy-type solution. This is due to the reason that each Levy-type plate element has only a pair of line nodes on opposite edges, which limits its application to plate assemblies only in a one-directional manner. In the current S-DSM, each plate element has four line nodes at disposal for the assembly in a much more general manner. This flexibility contributes to the versatility of the current S-DSM enormously. With such analytically formulated DS elements, one can model complex structures accurately by plate assemblies.

For the sake of illustration, Fig. 3 shows the assembly procedure for a simple L-shaped plate. The L-shaped plate is modelled using three plate elements ①, ②, and ③ with ten line nodes numbered therein. The local DS matrices for the elements ①, ②, and ③ are denoted by blue □, red ○ and black △ blocks respectively. The assembly of the global DS matrix $\boldsymbol{K}_f$ of the final structure, which relates the force $\boldsymbol{f}_f$ to the displacement $\boldsymbol{d}_f$ Fourier coefficient vectors, is schematically shown on the right hand side of Fig. 3. Note that the two overlapped symbols denote the two common line nodes 3 and 5. It can be easily seen from this illustrative example that the assembly procedure is as simple as that of the FEM. Thus existing computer code available for FEM assembly can be used in the current S-DSM method directly or by making some minor modifications.

4.2. Application of arbitrarily prescribed boundary conditions

This section will show the implementation of arbitrarily prescribed boundary conditions to a plate assembly (with a single plate as a special case).

The boundary conditions can be arbitrarily prescribed on plate edges, which are directly transformed into vector form $\boldsymbol{f}_f$ and $\boldsymbol{d}_f$ as in Eq. (32) by using the modified Fourier series of Eq. (A.3). For instance, if the displacement boundary condition $W_i(\xi)$ is prescribed along the ith boundary $\xi \in [-L, L]$, by applying the modified Fourier series formula of Eq. (A.3), one can write

$$W_i(\xi) = \sum_{\substack{s\in\mathbb{N}\\ l\in\{0,1\}}} W_{ils} \cdot \frac{\mathcal{T}_l(\gamma_{ls}\xi)}{\sqrt{\zeta_{ls}L}}, \quad W_{ils} = \int_{-L}^{L} W_i(\xi)\frac{\mathcal{T}_l(\gamma_{ls}\xi)}{\sqrt{\zeta_{ls}L}}\mathrm{d}\xi \tag{40}$$

where the notations are defined in Table A.1 of Appendix A. By putting the Fourier coefficients into vector form one will have the displacement vector as: $[\boldsymbol{W}_i^0, \boldsymbol{W}_i^1]^T = [W_{i00}, W_{i01}, W_{i02}, \cdots, W_{i10}, W_{i11}, W_{i12}, \cdots]^T$, with $\boldsymbol{W}_i^0$ and $\boldsymbol{W}_i^1$ denoting respectively the symmetric and the antisymmetric components of displacements W_i. In this way, any arbitrarily prescribed boundary conditions such as line and/or point supports on the boundaries can be represented by the Fourier coefficient vectors $\boldsymbol{f}_f$ or $\boldsymbol{d}_f$. Moreover, the present method also benefits the application of elastic edge constraints which are another type of boundary conditions encountered in many real applications. There are generally two types of elastic edge constraints for the Kirchhoff plate theory, namely, the linear and the rotational elastic constraints. These constraints usually can be expressed in the following forms

$$K_x W = V_x, \quad R_x\phi_x = M_x, \qquad \text{along boundary} \quad x = x_{\mathcal{B}}, \tag{41a}$$

$$K_y W = V_y, \quad R_y\phi_y = M_y, \qquad \text{along boundary} \quad y = y_{\mathcal{B}}. \tag{41b}$$

Here, K_x and K_y are the linear spring constants along the corresponding boundaries, whereas R_x and R_y are the rotational spring constants. Expressing both sides of Eq. (41) in terms of the modified Fourier series formula of Eq. (A.3) will lead to the DS matrices of the spring constraints on the plate edges. The DS matrices of elastic edge restraints are then superposed to the unmodified DS matrix of the plate structure (i.e., without elastic constraints) to form the final DS matrix of the elastically constrained structural system. Similarly, the above procedure can be applied to model composite stiffened panels. A panel can be idealised as S-DS plate elements which are assembled at the location of stiffeners. The stiffeners are modelled as beam elements whose displacement (rotation) and force (moment), i.e., the related values for plate are W, ϕ, V and M, can be expressed by the modified Fourier series such as in Eq. (40). Finally, the S-DS matrix for the stiffener can be developed based on beam theories which can be directly superposed to the unmodified DS matrix of the plate structure. This is quite similar to the procedure for modelling elastic constraints given in Eq. (41).

Now it is appropriate to point out that the current S-DSM has also the advantages that are analogous to the boundary element method (BEM) [47–49], but free from its shortcomings. In the BEM, the fundamental solution is derived analytically or semi-analytically from the GDE which is then used to formulate the boundary integral equation (BIE). As a result, any boundary conditions in BEM can be applied and the BIE can be solved numerically. The current S-DSM is, in this aspect, similar to that of BEM. The DS formulation satisfies the GDE rigorously because it has been derived from the exact general solution. This formulation also provides the flexibility to apply any arbitrary boundary conditions.

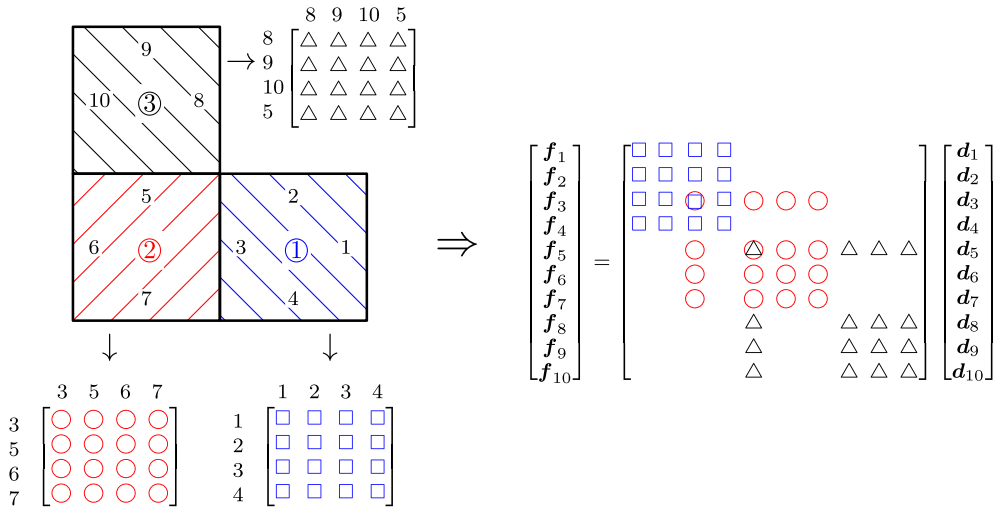

Fig. 3. Illustration of the assembly procedure of a L-shaped plate assembly.

However, unlike the conceptual complexity and the need to solve the BIE numerically as in BEM, the current S-DSM describes arbitrarily prescribed BC accurately and efficiently by modified Fourier series whose coefficients are related directly by the DS matrix.

After describing the prescribed boundary conditions in their Fourier coefficient form, it should be noted that there will generally be some cases where the displacement vectors of certain boundaries have zero vectors. A simple example is the classical boundary conditions for which the displacement corresponding to a certain plate edge can be zero. Therefore, the corresponding sub-vectors will be null. Usually, there are two methods for the implementation of such zero displacement boundary conditions. One is the penalty method and the other is the condensation method, see for example [19]. In the former, a sufficiently large stiffness can be added to the appropriate leading diagonal term to suppress the corresponding displacements whereas in the latter the rows and columns relating to the zero displacements are removed from the overall DS matrix of the complete structure. Understandably, the condensation method is superior to the penalty method in terms of accuracy and efficiency, but it involves some additional programming efforts. A brief description of the two techniques is given below.

Penalty method [50] is widely used to satisfy essential boundary conditions when finding eigenvalues of continuous systems. This has been proved to be a stable and satisfactory method, particularly when applying the Wittrick–Williams algorithm [11,12,14,15,51]. In the current S-DSM, the aforementioned elastic edge constraints directly facilitate the application of the penalty method, with the elastic constants $K_x,\ K_y,\ R_x,\ R_y$ of Eq. (41) being the penalty parameters. Therefore, a geometric constraint can be considered as an elastic constraint with $K_x(K_y)$ or/and $R_x(R_y)$ taking large enough value(s). The following boundary conditions on the ith edge of a plate can be applied: (i) Free (F): no penalty is applied, (ii) Simply supported (S): $\boldsymbol{W}_i$ is penalised, (iii) Clamped (C): both $\boldsymbol{W}_i$ and $\boldsymbol{\Phi}_i$ are penalised. Although the penalty method is quite reliable and fairly straightforward to apply, it has some shortcomings. The first drawback lies in the difficulty to determine a suitable magnitude for the penalty parameters: too small will lead to accuracy loss; too large may cause ill-conditioning or large round off errors [50]. Additionally, this technique does not reduce the size of the overall DS matrix and is therefore, not expected to reduce the computation cost.

The other technique is based on condensing the DS matrix. The rows and columns of the DS matrix corresponding to the DOF with zero displacement are removed in this method. Suppose that the displacement vector $\boldsymbol{d}_f$ can be partitioned into two sub-vectors $\boldsymbol{d}_a$ and $\boldsymbol{d}_b$ such that the displacement sub-vector $\boldsymbol{d}_b$ (corresponding to $\boldsymbol{f}_b$) and the force sub-vector $\boldsymbol{f}_a$ (corresponding to $\boldsymbol{d}_a$) are zero for the prescribed boundary conditions, then Eq. (38) can be recast in the following form

$$\begin{bmatrix} \boldsymbol{0} \\ \boldsymbol{f}_b \end{bmatrix} = \begin{bmatrix} \boldsymbol{K}_{aa} & \boldsymbol{K}_{ab} \\ \boldsymbol{K}_{ba} & \boldsymbol{K}_{bb} \end{bmatrix} \begin{bmatrix} \boldsymbol{d}_a \\ \boldsymbol{0} \end{bmatrix} \tag{42}$$

where $\boldsymbol{K}_{ab} = \boldsymbol{K}_{ba}^T$. In such cases, Eq. (42) is condensed to

$$\boldsymbol{K}_{aa}\boldsymbol{d}_a = \boldsymbol{0}. \tag{43}$$

Thus the natural frequencies can be computed by applying the WW algorithm to the above condensed DS matrix $\boldsymbol{K}_{aa}$. Even though this condensation technique is not as easy as the penalty method, it certainly avoids any possible loss of accuracy. More importantly, it condenses the DS matrix and therefore reduces the computational cost. Therefore, in the current S-DSM, the condensation method is applied in stead of the penalty method.

Having applied the prescribed boundary conditions to formulate the overall DS matrix $\boldsymbol{K}_f$, the natural frequencies and mode shapes computation of the plate structure follows from the application of the Wittrick–Williams algorithm [3], which is explained in the next section.

5. The Wittrick–Williams algorithm enhancement and mode shape computation

The overall dynamic stiffness (DS) matrix $\boldsymbol{K}_f$ for the final structure with prescribed constraints is essentially used for an accurate and efficient free vibration analysis. A reliable method to achieve this is to apply the well-known Wittrick–Williams (WW) algorithm [3]. The algorithm monitors the Sturm sequence properties of $\boldsymbol{K}_f$ in such a way that there is no possibility of missing any natural frequency of the structure. This is, of course, impossible in most analytical and approximate methods. It should be emphasised that some difficulties may arise in the WW algorithm application, but for the current problem potential stumbling blocks have been removed so as to make the current S-DSM reliable, computationally efficient and accurate.

5.1. Basic features and enhancement

Suppose that ω denotes the circular (or angular) frequency of a vibrating structure, then according to the WW algorithm, as ω is increased from zero to ω^*, the number of natural frequencies passed (J) is given by

$$J = J_0 + s\{\boldsymbol{K}_f\}, \tag{44}$$

where $\boldsymbol{K}_f$, the overall DS matrix of the final structure whose elements depend on ω is evaluated at $\omega = \omega^*$; $s\{\boldsymbol{K}_f\}$ is the number of negative elements on the leading diagonal of $\boldsymbol{K}_f^{\triangle}$, and $\boldsymbol{K}_f^{\triangle}$ is the upper triangular matrix obtained by applying the usual form of Gauss elimination to $\boldsymbol{K}_f$, and J_0 is the number of natural frequencies of the structure still lying between $\omega = 0$ and $\omega = \omega^*$ when the displacement components to which $\boldsymbol{K}_f$ corresponds are all zeros. Thus

$$J_0 = \sum J_m, \tag{45}$$

where J_m is the number of natural frequencies between $\omega = 0$ and $\omega = \omega^*$ for an individual component member with its boundaries fully clamped, while the summation extends over all structural members. Thus, with the knowledge of Eqs. (44) and (45), one can ascertain how many natural frequencies of a structure lie below an arbitrarily chosen trial frequency ω^*. This simple feature of the algorithm can be used to converge upon any required natural frequency to any desired accuracy.

Clearly, J_0 count is an essential part of the algorithm. However, the evaluation of J_0 count can sometimes be a difficult task and may become a potential drawback when applying the algorithm. In the literature, most of the previous DS methods on plates [11,12,15] use a sufficiently fine mesh to avoid J_0 computation i.e., to ensure that $J_0 \equiv 0$ for the entire frequency range of interest. However, this will no doubt increase the computational time. This is particularly true for the current S-DSM because a finer mesh will increase the number of DOFs much more significantly than that in a Levy-type plate DS theory. To meet this challenge, an efficient and reliable strategy is applied which is based on applying the WW algorithm in reverse to obtain J_m of Eq. (45) such that

$$J_m = J_S - s(\boldsymbol{K}_S), \tag{46}$$

where J_S is the overall sign count of a plate with all edges simply supported and $s(\boldsymbol{K}_S)$ is the sign count of its formulated DS matrix $\boldsymbol{K}_S$. The technique in Eq. (46) has been successfully applied to beam elements [52,53]. However, when it comes to plate problems it

becomes quite complicated and has not been applied in previous publications [11,12,15] with the lone exception of Ref. [10] (in which the J_S was formulated easily because the matrix $\boldsymbol{K}_S$ was a 2×2 matrix only). In the present method, the strategy based on Eq. (46) has been successfully implemented through several novel techniques.

First the computation of J_S in Eq. (46) is accomplished in an analytical manner by using the number theory. It is well-known that the exact solution for the natural frequency of an all-round simply supported cross-ply laminated Kirchhoff plate follows from the well-established Navier solution [44]. The natural frequency $\omega_{\hat{m}\hat{n}}$ for this case can be expressed analytically in the following form

$$\frac{(2a)^4 I_0 \omega_{\hat{m}\hat{n}}^2}{\pi^4 D_{11}} = \frac{\hat{m}^4 + \Pi_1 \hat{m}^2 \hat{n}^2 + \Pi_2 \hat{n}^4}{1 + \Pi_3 (\hat{m}^2 + \eta^2 \hat{n}^2)}, \quad \hat{m},\ \hat{n} \in \{1, 2, 3, \ldots\}, \tag{47}$$

where the left hand side of the equation is nondimensionalised and

$$\eta = \frac{a}{b}, \quad \Pi_1 = 2\Gamma\eta^2, \quad \Pi_2 = \Lambda\eta^4, \quad \Pi_3 = \frac{I_2}{I_0}\left(\frac{\pi}{2a}\right)^2. \tag{48}$$

Thus, J_S, the number of natural frequencies lying below a trial natural frequency ω^*, is essentially the number of pairs of $\hat{m}$ and $\hat{n}$ such that the left-hand side of Eq. (47) with $\omega_{\hat{m}\hat{n}} = \omega^*$ is greater than the right-hand side. Obviously, this can be obtained from a numerical search which may be computationally expensive and the procedure may miss some of the natural frequencies. However, there exists an analytical expression for J_S if one recognises that this problem is essentially an extension of the analytical number theory problem called *Gauss circle problem* [21] according to which

$$J_S = \sum_{\hat{m}=1}^{\lfloor \Pi_4 \rfloor} \lfloor \hat{n}^*(\hat{m}, \omega^*) \rfloor, \tag{49}$$

where

$$\Pi_4 = \frac{2a}{\pi}\sqrt[4]{\frac{I_0 \omega^{*2}}{D_{11}}}, \quad \hat{n}^*(\hat{m}, \omega^*) = \sqrt{\frac{\sqrt{\Pi_5^2 - 4\Pi_2\Pi_6} - \Pi_5}{2\Pi_2}},$$
$$\Pi_5 = \Pi_1 \hat{m}^2 - \Pi_3 \Pi_4^4 \eta^2, \quad \Pi_6 = \hat{m}^2(\hat{m}^2 - \Pi_3 \Pi_4^4)$$

and '$\lfloor \cdot \rfloor$' is the floor function denoting the largest integer not greater than '$\cdot$'. The detailed mathematical proof of the above expression is not given here due to brevity.

Next, the computation of $s(\boldsymbol{K}_S)$ in Eq. (46) is achieved in an elegant way by taking advantage of the mixed-variable formulation explained earlier in Section 3.1. It is well-known that when a geometrically symmetric structure is subject to symmetric constraints, the displacement field will be either symmetric or antisymmetric. Therefore, in the present case where a rectangular plate is subjected to all round simple supports, the four symmetric/antisymmetric DS matrices are decoupled to describe the deformation with corresponding symmetric/antisymmetric properties in the frequency domain. Hence, $s(\boldsymbol{K}_S) = \sum_{k,j\in\{0,1\}} s(\boldsymbol{K}_S^{kj})$. Now recalling Eq. (31), the case with fully simple supports becomes equivalent to letting $\boldsymbol{M}^{kj} = \boldsymbol{W}^{kj} = \boldsymbol{0}$, such that $s(\boldsymbol{K}_S^{kj}) = s(\boldsymbol{A}_{M\Phi}^{kj} - \boldsymbol{A}_{MV}^{kj}\boldsymbol{A}_{WV}^{kj\ -1}\boldsymbol{A}_{W\Phi}^{kj})$. In this way, one has

$$s(\boldsymbol{K}_S) = \sum_{k,j\in\{0,1\}} s(\boldsymbol{A}_{M\Phi}^{kj} - \boldsymbol{A}_{MV}^{kj}\boldsymbol{A}_{WV}^{kj\ -1}\boldsymbol{A}_{W\Phi}^{kj}). \tag{50}$$

The above technique of computing J_S and $s(\boldsymbol{K}_S)$ resolves completely the problem of determining J_0 in a highly efficient, accurate and reliable manner.

5.2. Mode shape computation

The mode shape computation in the current S-DSM is somehow different from the classical DSM approach due to the application of the condensation method when applying the BC. Here the following steps are used.

(1) Substitute the computed eigenvalues in the condensed matrix for the whole system $\boldsymbol{K}_{aa}$ of Eq. (43) and then assign an arbitrary value to a chosen DOF of $\boldsymbol{d}_a$ to determine the rest of the values in the displacement vector in terms of the chosen one by solving the algebraic system.
(2) Collect the condensed displacement vector $\boldsymbol{d}_a$ and the zero displacement vector together, which is essentially an inverse procedure of the condensation method as evident from Eq. (42).
(3) Decompose the displacement vector $\boldsymbol{d}_f$ of the whole structure into that of plate element $\boldsymbol{d}$ following an inverse step of the assembly procedure described in Section 4.1.
(4) For each plate element, the displacement vectors $\boldsymbol{d}^{kj}$ can be obtained from $\boldsymbol{d}$ according to Eq. (37) following which $\boldsymbol{K}^{kj}$ and $\boldsymbol{f}^{kj}$ are computed from Eq. (31).
(5) The unknown coefficients A_{km} and B_{jn} for each kj component are calculated using Eqs. (27) and (28) which are substituted into Eq. (15) and finally into Eq. (14) to recover the mode shapes in an analytical manner.

6. Conclusions

In this Part I of the two-part paper, a novel spectral-dynamic stiffness method (S-DSM) has been developed for free flexural vibration analysis of orthotropic composite plates and their assemblies with arbitrary boundary conditions. This research has removed previous restrictions on DS theories of plate structures. The other related main contributions made in this paper are: (i) Some important mathematical techniques such as modified Fourier series are utilised to keep the symplecticity of the DS formulation of the Hamiltonian system, (ii) With the aid of spectral idea, the ensuing DS matrix has been shown to have complete flexibility to accommodate arbitrarily prescribed boundary conditions, (iii) The assembly procedure of composite plate assemblies has been developed and fully explained, (iv) The DS matrix was formulated through an intensively symbolic and yet simplified way with clear physical interpretation, which is capable of handling complex plate structures and (v) Several novel techniques have been proposed, which have resolved the sign count of a fully-clamped plate leading to the well-known J_0 term. This is a significant enhancement to the Wittrick–Williams algorithm to make it robust and efficient within all frequency range covering low to high values.

In the second part of this paper [54], the current S-DSM is applied to a wide range of plated structures made of composite materials. The results obtained are compared with the results from other analytical methods as well as those computed by the commercial finite element package ABAQUS. It is demonstrated that the S-DSM is superior to any other analytical or numerical known methods in terms of the exactness, efficiency and versatility.

Acknowledgments

The authors appreciate the support given by EPSRC (UK) through a Grant EP/J007706/1 which made this research possible. The authors are also grateful to Prof. Stanislav Papkov (Sevastopol National Technical University) for many stimulating discussions.

Table A.1
The first four trigonometric functions. When applied to Eq. (9), the notations are adopted as either $\xi = x,\ l = k,\ s = m,\ \gamma_{ls} = \alpha_{km},\ L = a$ or $\xi = y,\ l = j,\ s = n,\ \gamma_{ls} = \beta_{jn},\ L = b$.

$\mathcal{T}_l(\gamma_{ls}\xi)$	l	$s=0$	$s=1$	$s=2$	$s=3$
$\cos\gamma_{ls}\xi$	0	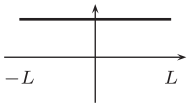	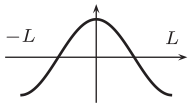	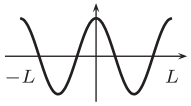	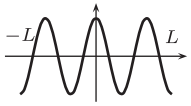
$\sin\gamma_{ls}\xi$	0	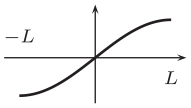	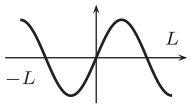	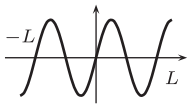	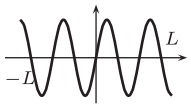

Appendix A. Modified Fourier basis function and the corresponding modified Fourier series

The set of modified Fourier basis functions adopted in the formulation to represent any arbitrary continuous 1D function is of the form

$$\mathcal{T}_l(\gamma_{ls}\xi) = \begin{cases} \cos(\frac{s\pi}{L}\xi) & l=0 \\ \sin\left((s+\frac{1}{2})\frac{\pi}{L}\xi\right) & l=1 \end{cases}, \quad \xi\in[-L,L], \quad s\in\mathbb{N}, \tag{A.1}$$

where $\mathbb{N}=\{0,1,2,\ldots\}$ is the non-negative integer set. It can be proved that the above basis functions form a complete orthogonal set. Note that the wave number γ_{ls} of the cosine/sine basis functions are to be carefully chosen to provide the flexibility to describe any arbitrary 1D function with arbitrary boundary conditions at its boundaries $\xi=\pm L$. This is illustrated in Table A.1, where the first four cosine/sine functions are shown. Furthermore, due to the wavenumber adopted in Eq. (A.1), one has

$$\left.\frac{\mathrm{d}^i\mathcal{T}_l(\gamma_{ls}\xi)}{\mathrm{d}\xi^i}\right|_{\xi=L} = \begin{cases} (-1)^{s+i/2}\gamma_{ls}^i & i \text{ is even} \\ 0 & i \text{ is odd} \end{cases}. \tag{A.2}$$

There are different adaptations of Fourier series in common use, see for example Ref. [55]. In this paper, the following modified Fourier series related to the basis functions defined in Eq. (A.1) is utilised in which the dependence on the length of the integral range $[-L,L]$ is eliminated. For any arbitrary displacement or force boundary condition $f(\xi)$ along a plate edge $\xi\in[-L,L]$, one can write

$$f(\xi) = \sum_{\substack{s\in\mathbb{N}\\ l\in\{0,1\}}} F_{ls}\cdot\frac{\mathcal{T}_l(\gamma_{ls}\xi)}{\sqrt{\zeta_{ls}L}}, \quad F_{ls} = \int_{-L}^{L} f(\xi)\frac{\mathcal{T}_l(\gamma_{ls}\xi)}{\sqrt{\zeta_{ls}L}}\mathrm{d}\xi, \tag{A.3}$$

where $s\in\mathbb{N}$ and

$$\zeta_{ls} = \begin{cases} 2 & l=0 \text{ and } s=0 \\ 1 & l=1 \text{ or } s\geqslant 1 \end{cases}. \tag{A.4}$$

Note that $\sqrt{\zeta_{ls}L}$ appearing in Eq. (A.3) provides the symmetry of the forward and inverse Fourier transformation. The above technique is for the purpose of retaining the symplecticity of the formulated system.

Based on Eq. (A.3), the hyperbolic functions in Eq. (16) can be transformed into Fourier series as follows:

$$\mathcal{H}_j(py) = \sum_{n\in\mathbb{N}}\frac{2(-1)^n p\mathcal{H}_j^*(pb)}{\sqrt{\zeta_{jn}b}(p^2+\beta_{jn}^2)}\cdot\frac{\mathcal{T}_j(\beta_{jn}y)}{\sqrt{\zeta_{jn}b}} \tag{A.5a}$$

$$\mathcal{H}_k(qx) = \sum_{m\in\mathbb{N}}\frac{2(-1)^m q\mathcal{H}_k^*(qa)}{\sqrt{\zeta_{km}a}(q^2+\alpha_{km}^2)}\cdot\frac{\mathcal{T}_k(\alpha_{km}x)}{\sqrt{\zeta_{km}a}}, \tag{A.5b}$$

where p and q stand for p_{1km}, p_{2km} and q_{1jn}, q_{2jn}, respectively, and ζ_{jn}, ζ_{km} and $\mathcal{H}_j^*(pb)$, $\mathcal{H}_k^*(qa)$ follow the definitions given in Eqs. (A.4) and (18) receptively.

Appendix B. The relationship between arbitrary boundary conditions and their *kj* components

Considering the symmetry/antisymmetry of W^{kj} of Eq. (15) and its derivatives, the relationships between the boundary conditions (BC) in Eq. (21) and their four components in Eq. (22) are as follows

$$\begin{bmatrix} W_1 \\ \phi_1 \\ W_2 \\ \phi_2 \\ W_3 \\ \phi_3 \\ W_4 \\ \phi_4 \end{bmatrix} = \begin{bmatrix} W_a^{00}+W_a^{01}+W_a^{10}+W_a^{11} \\ \phi_a^{00}+\phi_a^{01}+\phi_a^{10}+\phi_a^{11} \\ W_b^{00}+W_b^{01}+W_b^{10}+W_b^{11} \\ \phi_b^{00}+\phi_b^{01}+\phi_b^{10}+\phi_b^{11} \\ W_a^{00}+W_a^{01}-W_a^{10}-W_a^{11} \\ -\phi_a^{00}-\phi_a^{01}+\phi_a^{10}+\phi_a^{11} \\ W_b^{00}-W_b^{01}+W_b^{10}-W_b^{11} \\ -\phi_b^{00}+\phi_b^{01}-\phi_b^{10}+\phi_b^{11} \end{bmatrix}, \quad \begin{bmatrix} V_1 \\ M_1 \\ V_2 \\ M_2 \\ V_3 \\ M_3 \\ V_4 \\ M_4 \end{bmatrix} = \begin{bmatrix} V_a^{00}+V_a^{01}+V_a^{10}+V_a^{11} \\ M_a^{00}+M_a^{01}+M_a^{10}+M_a^{11} \\ V_b^{00}+V_b^{01}+V_b^{10}+V_b^{11} \\ M_b^{00}+M_b^{01}+M_b^{10}+M_b^{11} \\ V_a^{00}+V_a^{01}-V_a^{10}-V_a^{11} \\ -M_a^{00}-M_a^{01}+M_a^{10}+M_a^{11} \\ V_b^{00}-V_b^{01}+V_b^{10}-V_b^{11} \\ -M_b^{00}+M_b^{01}-M_b^{10}+M_b^{11} \end{bmatrix}. \tag{B.1}$$

It should be noted that any prescribed BC on the left-hand sides of Eq. (B.1) can be decomposed into a symmetric and an antisymmetric components, e.g., $W_i = W_i^0 + W_i^1$ and $V_i = V_i^0 + V_i^1$ with subscript '0' or '1' denoting the symmetric or the antisymmetric component respectively. If the decomposition is applied to all the entries on the left-hand side vectors in Eq. (B.1) and equated to the symmetric/antisymmetric components of both sides of Eq. (B.1) separately, the following relationships for the displacement BC of the quarter plate and the entire plate can be obtained. Thus

$$\left[W_1^0, W_1^1, W_3^0, W_3^1\right]^T = \boldsymbol{T}_1[W_a^{00}, W_a^{01}, W_a^{10}, W_a^{11}]^T \tag{B.2a}$$

$$\left[W_2^0, W_2^1, W_4^0, W_4^1\right]^T = \boldsymbol{T}_2[W_b^{00}, W_b^{01}, W_b^{10}, W_b^{11}]^T \tag{B.2b}$$

$$\left[\phi_1^0, \phi_1^1, \phi_3^0, \phi_3^1\right]^T = \boldsymbol{T}_3[\phi_a^{00}, \phi_a^{01}, \phi_a^{10}, \phi_a^{11}]^T \tag{B.2c}$$

$$\left[\phi_2^0, \phi_2^1, \phi_4^0, \phi_4^1\right]^T = \boldsymbol{T}_4[\phi_b^{00}, \phi_b^{01}, \phi_b^{10}, \phi_b^{11}]^T. \tag{B.2d}$$

The relationships between the corresponding force BC are

$$\left[V_1^0, V_1^1, V_3^0, V_3^1\right]^T = \boldsymbol{T}_1\left[V_a^{00}, V_a^{01}, V_a^{10}, V_a^{11}\right]^T \tag{B.3a}$$

$$\left[V_2^0, V_2^1, V_4^0, V_4^1\right]^T = \boldsymbol{T}_2\left[V_b^{00}, V_b^{01}, V_b^{10}, V_b^{11}\right]^T \tag{B.3b}$$

$$\left[M_1^0, M_1^1, M_3^0, M_3^1\right]^T = \boldsymbol{T}_3\left[M_a^{00}, M_a^{01}, M_a^{10}, M_a^{11}\right]^T \tag{B.3c}$$

$$\left[M_2^0, M_2^1, M_4^0, M_4^1\right]^T = \boldsymbol{T}_4\left[M_b^{00}, M_b^{01}, M_b^{10}, M_b^{11}\right]^T. \tag{B.3d}$$

In Eqs. (B.2) and (B.3), $\boldsymbol{T}_\tau(\tau=1,2,3,4)$ are transfer matrices defined as

$$\boldsymbol{T}_1 = \begin{bmatrix} 1 & 0 & 1 & 0 \\ 0 & 1 & 0 & 1 \\ 1 & 0 & -1 & 0 \\ 0 & 1 & 0 & -1 \end{bmatrix}, \quad \boldsymbol{T}_2 = \begin{bmatrix} 1 & 1 & 0 & 0 \\ 0 & 0 & 1 & 1 \\ 1 & -1 & 0 & 0 \\ 0 & 0 & 1 & -1 \end{bmatrix}, \tag{B.4a}$$

$$\boldsymbol{T}_3 = \begin{bmatrix} 1 & 0 & 1 & 0 \\ 0 & 1 & 0 & 1 \\ -1 & 0 & 1 & 0 \\ 0 & -1 & 0 & 1 \end{bmatrix}, \quad \boldsymbol{T}_4 = \begin{bmatrix} 1 & 1 & 0 & 0 \\ 0 & 0 & 1 & 1 \\ -1 & 1 & 0 & 0 \\ 0 & 0 & -1 & 1 \end{bmatrix}. \tag{B.4b}$$

Interestingly, it can be shown that

$$\boldsymbol{T}_\tau^{-1} = \boldsymbol{T}_\tau^T/2. \tag{B.5}$$

It is therefore straightforward to represent the vectors on the right-hand side of Eqs. (B.2) and (B.3) by the left-hand side vectors. For example

$$\left[W_a^{00}, W_a^{01}, W_a^{10}, W_a^{11}\right]^T = \boldsymbol{T}_1^T\left[W_1^0, W_1^1, W_3^0, W_3^1\right]^T/2. \tag{B.6}$$

Appendix C. Infinite system of algebraic equations stemming from W_a^{kj}, W_b^{kj}, M_a^{kj} and M_b^{kj} of Eq. (22)

By equating the expressions of W_a^{kj}, W_b^{kj} in Eqs. (22) and (23), the following two relationships are obtained

$$\begin{aligned} W^{kj}\Big|_{x=a} &= \sum_{m\in\mathbb{N}}(-1)^m\left[A_{1km}\mathcal{H}_j(p_{1km}y) + A_{2km}\mathcal{H}_j(p_{2km}y)\right] \\ &\quad + \sum_{n\in\mathbb{N}}\left[B_{1jn}\mathcal{H}_k(q_{1jn}a) \quad + B_{2jn}\mathcal{H}_k(q_{2jn}a)\right]\mathcal{T}_j(\beta_{jn}y) \\ &= \sum_{n\in\mathbb{N}} W_{ajn}\mathcal{T}_j(\beta_{jn}y)/\sqrt{\zeta_{jn}b} \end{aligned} \tag{C.1a}$$

$$\begin{aligned} W^{kj}\Big|_{y=b} &= \sum_{n\in\mathbb{N}}(-1)^n\left[B_{1jn}\mathcal{H}_k(q_{1jn}x) + B_{2jn}\mathcal{H}_k(q_{2jn}x)\right] \\ &\quad + \sum_{m\in\mathbb{N}}\left[A_{1km}\mathcal{H}_j(p_{1km}b) \quad + A_{2km}\mathcal{H}_j(p_{2km}b)\right]\mathcal{T}_k(\alpha_{km}x) \\ &= \sum_{m\in\mathbb{N}} W_{bkm}\mathcal{T}_k(\alpha_{km}x)/\sqrt{\zeta_{km}a}. \end{aligned} \tag{C.1b}$$

Substituting Eqs. (27) and (28) into Eq. (C.1), applying the Fourier series Eq. (A.5) to the hyperbolic functions $\mathcal{H}_j(p_{1km}y)$, $\mathcal{H}_j(p_{2km}y)$, $\mathcal{H}_k(q_{1jn}x)$ and $\mathcal{H}_k(q_{2jn}x)$, and eliminating the common terms $\mathcal{T}_j(\beta_{jn}y)/\sqrt{\zeta_{jn}b}$ or $\mathcal{T}_k(\alpha_{km}x)/\sqrt{\zeta_{km}a}$ from both sides, the following infinite algebraic system arises

$$\begin{aligned} W_{ajn} &= \sum_{m\in\mathbb{N}}\frac{2(-1)^{m+n}\left[V_{bkm} - \left(\nu_{21}\alpha_{km}^2 + \Lambda\beta_{jn}^2\right)\phi_{bkm}\right]}{\sqrt{\zeta_{km}\zeta_{jn}ab}\Lambda(p_{1km}^2+\beta_{jn}^2)(p_{2km}^2+\beta_{jn}^2)} \\ &\quad + \frac{1}{q_{2jn}^2 - q_{1jn}^2}\left\{\left[V_{ajn} - \left(\nu_{21}\beta_{jn}^2 - q_{1jn}^2\right)\phi_{ajn}\right]\frac{\mathcal{TH}_k(q_{1jn}a)}{q_{1jn}}\right. \\ &\quad \left. - \left[V_{ajn} - \left(\nu_{21}\beta_{jn}^2 - q_{2jn}^2\right)\phi_{ajn}\right]\frac{\mathcal{TH}_k(q_{2jn}a)}{q_{2jn}}\right\} \end{aligned} \tag{C.2}$$

$$\begin{aligned} W_{bkm} &= \frac{1}{\Lambda(p_{2km}^2 - p_{1km}^2)}\left\{\left[V_{bkm} - (\nu_{21}\alpha_{km}^2 - \Lambda p_{1km}^2)\phi_{bkm}\right]\frac{\mathcal{TH}_j(p_{1km}b)}{p_{1km}}\right. \\ &\quad \left. - \left[V_{bkm} - (\nu_{21}\alpha_{km}^2 - \Lambda p_{2km}^2)\phi_{bkm}\right]\frac{\mathcal{TH}_j(p_{2km}b)}{p_{2km}}\right\} \\ &\quad + \sum_{n\in\mathbb{N}}\frac{2(-1)^{m+n}\left[V_{ajn} - \left(\alpha_{km}^2 + \nu_{21}\beta_{jn}^2\right)\phi_{ajn}\right]}{\sqrt{\zeta_{km}\zeta_{jn}ab}(q_{1jn}^2+\alpha_{km}^2)(q_{2jn}^2+\alpha_{km}^2)}, \end{aligned} \tag{C.3}$$

where the notation $\mathcal{TH}_l(\Xi) = \mathcal{H}_l(\Xi)/\mathcal{H}_l^*(\Xi)$ has been used. Similarly, when the already determined unknowns of Eqs. (27) and (28) and the Fourier series of Eq. (A.5) are substituted into the expressions of M_a^{kj}, M_b^{kj} in Eqs. (22) and (23), another set of infinite algebraic system can be obtained using an analogous procedure.

Appendix D. Expressions of the coefficient matrices in the mixed-variable formulation of Eq. (29)

The analytical expressions for the coefficient matrices in Eq. (29) are given in this appendix. After symbolic manipulation, the four coefficient matrices $\boldsymbol{A}_{W\Phi}^{kj}$, $\boldsymbol{A}_{WV}^{kj}$, $\boldsymbol{A}_{M\Phi}^{kj}$ and $\boldsymbol{A}_{MV}^{kj}$ can be expressed in an extremely concise form. The following expressions are the only analytical expressions required to model complex composite plate-like structures.

$$\boldsymbol{A}_{W\Phi}^{kj} = -\begin{bmatrix} \mathrm{diag}_n[(\Sigma_1\Upsilon_1 - \Sigma_2\Upsilon_2)/\Sigma_5] & [\Sigma_7\Sigma_9]_{n,m} \\ [\Sigma_8\Sigma_{10}]_{m,n} & \mathrm{diag}_m[(\Sigma_3\Upsilon_3 - \Sigma_4\Upsilon_4)/\Sigma_6] \end{bmatrix} \tag{D.1a}$$

$$\boldsymbol{A}_{WV}^{kj} = \begin{bmatrix} \mathrm{diag}_n[(\Upsilon_1 - \Upsilon_2)/\Sigma_5] & [\Sigma_7]_{n,m} \\ [\Sigma_8]_{m,n} & \mathrm{diag}_m[(\Upsilon_3 - \Upsilon_4)/\Sigma_6] \end{bmatrix} \tag{D.1b}$$

$$\boldsymbol{A}_{M\Phi}^{kj} = -\begin{bmatrix} \mathrm{diag}_n[(\Upsilon_1 - \Upsilon_2)/\Sigma_5] & [\Sigma_7]_{n,m} \\ [\Sigma_8]_{m,n} & \mathrm{diag}_m[(\Upsilon_3 - \Upsilon_4)/\Sigma_6] \end{bmatrix} \tag{D.1c}$$

$$\boldsymbol{A}_{MV}^{kj} = \begin{bmatrix} \mathrm{diag}_n[(\Sigma_1\Upsilon_1 - \Sigma_2\Upsilon_2)/\Sigma_5] & [\Sigma_7\Sigma_{10}]_{n,m} \\ [\Sigma_8\Sigma_9]_{m,n} & \mathrm{diag}_m[(\Sigma_3\Upsilon_3 - \Sigma_4\Upsilon_4)/\Sigma_6] \end{bmatrix} \tag{D.1d}$$

where

$$\begin{aligned} &\Upsilon_1 = \mathcal{H}_k(q_{1jn}a)/(\mathcal{H}_k^*(q_{1jn}a)q_{1jn}), && \Upsilon_2 = \mathcal{H}_k(q_{2jn}a)/(\mathcal{H}_k^*(q_{2jn}a)q_{2jn}), \\ &\Upsilon_3 = \mathcal{H}_j(p_{1km}b)/(\mathcal{H}_j^*(p_{1km}b)p_{1km}), && \Upsilon_4 = \mathcal{H}_j(p_{2km}b)/(\mathcal{H}_j^*(p_{2km}b)p_{1km}), \\ &\Sigma_1 = \nu_{21}\beta_{jn}^2 - q_{1jn}^2, && \Sigma_2 = \nu_{21}\beta_{jn}^2 - q_{2jn}^2, \\ &\Sigma_3 = \nu_{21}\alpha_{km}^2 - \Lambda p_{1km}^2, && \Sigma_4 = \nu_{21}\alpha_{km}^2 - \Lambda p_{2km}^2, \\ &\Sigma_5 = q_{2jn}^2 - q_{1jn}^2, && \Sigma_6 = \Lambda(p_{2km}^2 - p_{1km}^2), \\ &\Sigma_7 = 2(-1)^{m+n}/\left[\Lambda\sqrt{\zeta_{km}\zeta_{jn}ab}(p_{1km}^2+\beta_{jn}^2)(p_{2km}^2+\beta_{jn}^2)\right], \\ &\Sigma_8 = 2(-1)^{m+n}/\left[\sqrt{\zeta_{km}\zeta_{jn}ab}(q_{1jn}^2+\alpha_{km}^2)(q_{2jn}^2+\alpha_{km}^2)\right], \\ &\Sigma_9 = \nu_{21}\alpha_{km}^2 + \Lambda\beta_{jn}^2, && \Sigma_{10} = \alpha_{km}^2 + \nu_{21}\beta_{jn}^2, \\ &\Sigma_{11} = \alpha_{km}^2\beta_{jn}^2(\Lambda - 2\nu_{21}\Gamma + \nu_{21}^2) + \nu_{21}\left[\kappa + \chi(\alpha_{km}^2 + \beta_{jn}^2)\right]. \end{aligned}$$

where the hyperbolic functions $\mathcal{H}$ and $\mathcal{H}^*$ were defined in Eqs. (16) and (18) respectively. In Eq. (D.1), '$\mathrm{diag}_n[\cdot]$' represents a diagonal matrix whose diagonal terms are expressed by '$\cdot$' with the subscript n varying from 0 to ∞, whereas '$[\cdot]_{n,m}$' stands for a matrix whose entries are '$\cdot$' with n (row number) and m (column number) taking from 0 to ∞. Similarly, it is easy to understand the notations '$\mathrm{diag}_m[\cdot]$' and '$[\cdot]_{m,n}$'. If the series expansion is truncated with $n \in [0, N-1]$ and $m \in [0, M-1]$, then all of the four matrices in Eq. (D.1) are of size $(M+N)\times(M+N)$. Note that the notation $(\cdot)^{kj}$ with kj taking the values '00', '01', '10' and '11', implies that these definitions are for all of the four symmetric/antisymmetric components.

Clearly, the above analytical expressions carry physical meanings. For instance, Γ^*, Λ and ν_{21} are material parameters, χ is the rotatory inertia parameter (Note that $\chi = 0$ when rotatory inertia is ignored); α_{km}, β_{jn} are the wavenumbers and p_{1km}, p_{2km}, q_{1jn} and q_{2jn} are the frequency-dependent wave parameters. It is interesting to note that the two sub-matrices in the diagonal position for all of the four matrices in Eq. (D.1) are diagonal matrices. This is due to the fact that all of the frequency–wavenumber dependent DOF in one direction (for the corresponding displacements or forces) are orthogonal to each other. Also, it can be deduced from

Eq. (20) that $\Sigma_7 = \Sigma_8 = 2(-1)^{m+n} \Big/ \left\{ \sqrt{\zeta_{km}\zeta_{jn}}ab[\alpha_{km}^2(\alpha_{km}^2 + 2\Gamma\beta_{jn}^2) + \beta_{jn}^2(\Lambda\beta_{jn}^2 - \chi) - \kappa] \right\}$.

References

[1] Karniadakis GE, Sherwin SJ. Spectral/HP element methods for computational fluid dynamics. 2nd ed. Oxford, Oxford; 2005.
[2] Koloušek V. Anwendung des Gesetzes der virtuellen Verschiebungen und des Reziprozitätssatzes in der Stabwerksdynamik. Ingenieur-Archiv 1941;12(6):363–70. http://dx.doi.org/10.1007/BF02089894.
[3] Wittrick WH, Williams FW. A general algorithm for computing natural frequencies of elastic structures. Quart J Mech Appl Math 1971;XXIV(3):263–84. http://dx.doi.org/10.1093/qjmam/24.3.263.
[4] Banerjee JR, Williams FW. Exact Bernoulli–Euler static stiffness matrix for a range of tapered beam–columns. Int J Numer Meth Eng 1986;23:1615–28. http://dx.doi.org/10.1002/nme.1620230904.
[5] Banerjee JR, Fisher SA. Coupled bending-torsional dynamic stiffness matrix for axially loaded beam elements. Int J Numer Meth Eng 1992;33:739–51. http://dx.doi.org/10.1016/0020-7683(94)90075-2.
[6] Banerjee JR, Williams FW. Coupled bending-torsional dynamic stiffness matrix for Timoshenko beam elements. Comput Struct 1992;42(3):301–10. http://dx.doi.org/10.1016/0045-7949(92)90026-V.
[7] Banerjee JR, Williams FW. Coupled bending-torsional dynamic stiffness matrix of an axially loaded Timoshenko beam element. Int J Solids Struct 1994;31(6):749–62. http://dx.doi.org/10.1016/0020-7683(94)90075-2.
[8] Banerjee JR, Sobey AJ. Dynamic stiffness formulation and free vibration analysis of a three-layered sandwich beam. Int J Solids Struct 2005;42(8):2181–97. http://dx.doi.org/10.1016/j.ijsolstr.2004.09.013.
[9] Banerjee JR, Gunawardana WD. Dynamic stiffness matrix development and free vibration analysis of a moving beam. J Sound Vib 2007;303(1–2):135–43. http://dx.doi.org/10.1016/j.jsv.2006.12.020.
[10] Wittrick WH, Williams FW. Buckling and vibration of anisotropic or isotropic plate assemblies under combined loadings. Int J Mech Sci 1974;16(4):209–39. http://dx.doi.org/10.1016/0020-7403(74)90069-1.
[11] Boscolo M, Banerjee JR. Dynamic stiffness elements and their applications for plates using first order shear deformation theory. Comput Struct 2011;89(3–4):395–410. http://dx.doi.org/10.1016/j.compstruc.2010.11.005.
[12] Boscolo M, Banerjee JR. Dynamic stiffness formulation for composite Mindlin plates for exact modal analysis of structures. Part I: theory. Comput Struct 2012;96–97:61–73. http://dx.doi.org/10.1016/j.compstruc.2012.01.002.
[13] Boscolo M, Banerjee JR. Dynamic stiffness formulation for composite Mindlin plates for exact modal analysis of structures. Part II: results and applications. Comput Struct 2012;96–97:74–83. http://dx.doi.org/10.1016/j.compstruc.2012.01.003.
[14] Fazzolari FA, Boscolo M, Banerjee JR. An exact dynamic stiffness element using a higher order shear deformation theory for free vibration analysis of composite plate assemblies. Compos Struct 2013;96:262–78. http://dx.doi.org/10.1016/j.compstruct.2012.08.033.
[15] Boscolo M, Banerjee JR. Layer-wise dynamic stiffness solution for free vibration analysis of laminated composite plates. J Sound Vib 2014;333(1):200–27. http://dx.doi.org/10.1016/j.jsv.2013.08.031.
[16] Boyd JP. Chebyshev and Fourier spectral methods. 2nd ed. Dover Publications; 2001 [New].
[17] Kopriva DA. Implementing spectral methods for partial differential equations: algorithms for scientists and engineers scientific computation. New York: Springer; 2009.
[18] Patera AT. A spectral element method for fluid dynamics: laminar flow in a channel expansion. J Comput Phys 1984;54:468–88. http://dx.doi.org/10.1016/0021-9991(84)90128-1.
[19] Ostachowicz W, Kudela P, Krawczuk M, Zak A. Guided waves in structures for SHM: the time – domain spectral element method. New Delhi: Wiley; 2012.
[20] Lee U. Spectral element method in structural dynamics. Singapore: John Wiley & Sons; 2009.
[21] Hardy GH. Ramanujan: twelve lectures on subjects suggested by his life and work. 3rd ed. New York: AMS Chelsea Publishing; 1999.
[22] Ritz W. Theorie der Transversalschwingungen einer quadratischen Platte mit freien Rändern. Ann Phys 1909;333(4):737–86. http://dx.doi.org/10.1002/andp.19093330403.
[23] Leissa AW. The free vibration of rectangular plates. J Sound Vib 1973;31(3):257–93. http://dx.doi.org/10.1016/S0022-460X(73)80371-2.
[24] Bhat RB. Natural frequencies of rectangular plates using characteristic orthogonal polynomials in Rayleigh–Ritz method. J Sound Vib 1985;102(4):493–9. http://dx.doi.org/10.1016/S0022-460X(85)80109-7.
[25] Dozio L. On the use of the trigonometric Ritz method for general vibration analysis of rectangular Kirchhoff plates. Thin-Walled Struct 2011;49(1):129–44. http://dx.doi.org/10.1016/j.tws.2010.08.014.
[26] Li WL, Zhang X, Du J, Liu Z. An exact series solution for the transverse vibration of rectangular plates with general elastic boundary supports. J Sound Vib 2009;321(1–2):254–69. http://dx.doi.org/10.1016/j.jsv.2008.09.035.
[27] Khov H, Li WL, Gibson RF. An accurate solution method for the static and dynamic deflections of orthotropic plates with general boundary conditions. Compos Struct 2009;90(4):474–81. http://dx.doi.org/10.1016/j.compstruct.2009.04.020.
[28] Du J, Li WL, Liu Z, Yang T, Jin G. Free vibration of two elastically coupled rectangular plates with uniform elastic boundary restraints. J Sound Vib 2011;330(4):788–804. http://dx.doi.org/10.1016/j.jsv.2010.08.044.
[29] Xu H, Li WL, Du J. Modal analysis of general plate structures. J Vib Acoust 2013;136(2):021002. http://dx.doi.org/10.1115/1.4025876.
[30] Gorman DJ. Accurate free vibration analysis of clamped orthotropic plates by the method of superposition. J Sound Vib 1990;140(3):391–411. http://dx.doi.org/10.1016/0022-460X(90)90758-R.
[31] Gorman DJ. Accurate free vibration analysis of the completely free orthotropic rectangular plate by the method of superposition. J Sound Vib 1993;165(3):409–20. http://dx.doi.org/10.1006/jsvi.1993.1267.
[32] Kshirsagar S, Bhaskar K. Accurate and elegant free vibration and buckling studies of orthotropic rectangular plates using untruncated infinite series. J Sound Vib 2008;314(3–5):837–50. http://dx.doi.org/10.1016/j.jsv.2008.01.013.
[33] Kantorovich LV, Krylov VI. Approximate methods of higher analysis. Groningen: Noordhoff; 1958.
[34] Sakata T, Takahashi K, Bhat RB. Natural frequencies of orthotropic rectangular plates obtained by iterative reduction of the partial differential equation. J Sound Vib 1996;189(1):89–101. http://dx.doi.org/10.1006/jsvi.1996.9999.
[35] Dalaei M, Kerr A. Natural vibration analysis of clamped rectangular orthotropic plates. J Sound Vib 1996;189(3):399–406. http://dx.doi.org/10.1006/jsvi.1996.0026.
[36] Bercin AN. Free vibration solution for clamped orthotropic plates using the Kantorovich method. J Sound Vib 1996;196(2):243–7. http://dx.doi.org/10.1006/jsvi.1996.0479.
[37] Lekhnitskii SG. Elements of vibration analysis. New York: McGraw-Hill; 1986.
[38] Lamé MG. Leçons sur la théorie mathématique: de l'élasticité des corps solides. Paris: Bachelier; 1852.
[39] Gorman DJ, Yu SD. A review of the superposition method for computing free vibration eigenvalues of elastic structures. Comput Struct 2012;104–105:27–37. http://dx.doi.org/10.1016/j.compstruc.2012.02.018.
[40] Gorman DJ. Accurate free vibration analysis of the orthotropic cantilever plate. J Sound Vib 1995;181(4):605–18. http://dx.doi.org/10.1006/jsvi.1995.0161.
[41] Gorman DJ. Highly accurate free vibration eigenvalues for the completely free orthotropic plate. J Sound Vib 2005;280(3–5):1095–115. http://dx.doi.org/10.1016/j.jsv.2004.02.030.
[42] Gorman DJ, Singhal R. Free vibration analysis of cantilever plates with step discontinuities in properties by the method of superposition. J Sound Vib 2002;253(3):631–52. http://dx.doi.org/10.1006/jsvi.2001.4067.
[43] Gorman DJ, Garibaldi L. Accurate analytical type solutions for free vibration frequencies and mode shapes of multi-span bridge decks: the span-by-span approach. J Sound Vib 2006;290(1–2):321–36. http://dx.doi.org/10.1016/j.jsv.2005.03.020.
[44] Reddy JN. Mechanics of laminated composite plates and shells theory and analysis. 2nd ed. CRC Press; 2003.
[45] Doyle JF. Wave propagation in structures. 2nd ed. New York: Springer; 1997.
[46] Zhong WX. Duality system in applied mechanics and optimal control. London: Kluwer Academic Publishers; 2004.
[47] Gospodinov G, Ljutskanov D. The boundary element method applied to plates. Appl Math Model 1982;6:237–44. http://dx.doi.org/10.1016/S0307-904X(82)80031-0.
[48] Albuquerque EL, Sollero P, Fedelinski P. Free vibration analysis of anisotropic material structures using the boundary element method. Eng Anal Boundary Elem 2003;27(10):977–85. http://dx.doi.org/10.1016/S0955-7997(03)00074-2.
[49] Katsikadelis JT. The boundary element method for plate analysis. London: Elsevier; 2014.
[50] Ilanko S. Penalty methods for finding eigenvalues of continuous systems: emerging challenges and opportunities. Comput Struct 2012;104–105:50–4. http://dx.doi.org/10.1016/j.compstruc.2012.02.017.
[51] Ilanko S, Williams FW. Wittrick–Williams algorithm proof of bracketing and convergence theorems for eigenvalues of constrained structures with positive and negative penalty parameters. Int J Numer Meth Eng 2008;75:83–102. http://dx.doi.org/10.1002/nme.2247.
[52] Howson WP, Williams FW. Natural frequencies of frames with axially loaded Timoshenko members. J Sound Vib 1973;26(4):503–15. http://dx.doi.org/10.1016/S0022-460X(73)80216-0.
[53] Banerjee JR, Williams FW. Clamped–clamped natural frequencies of a bending-torsion coupled beam. J Sound Vib 1994;176(3):301–6. http://dx.doi.org/10.1006/jsvi.1994.1378.
[54] Liu X, Banerjee JR. An exact spectral-dynamic stiffness method for free flexural vibration analysis of orthotropic composite plate assemblies – part II: applications. Comput Struct 2015;132:1288–302. http://dx.doi.org/10.1016/j.compstruct.2015.07.020.
[55] Bracewell RN. The Fourier transform and its applications. 2nd ed. London: McGraw-Hill Book Company; 1978.